iScience

CellPress
OPEN ACCESS

Article

Decoding sunitinib resistance in ccRCC: Metabolic-reprogramming-induced ABAT and GABAergic system shifts

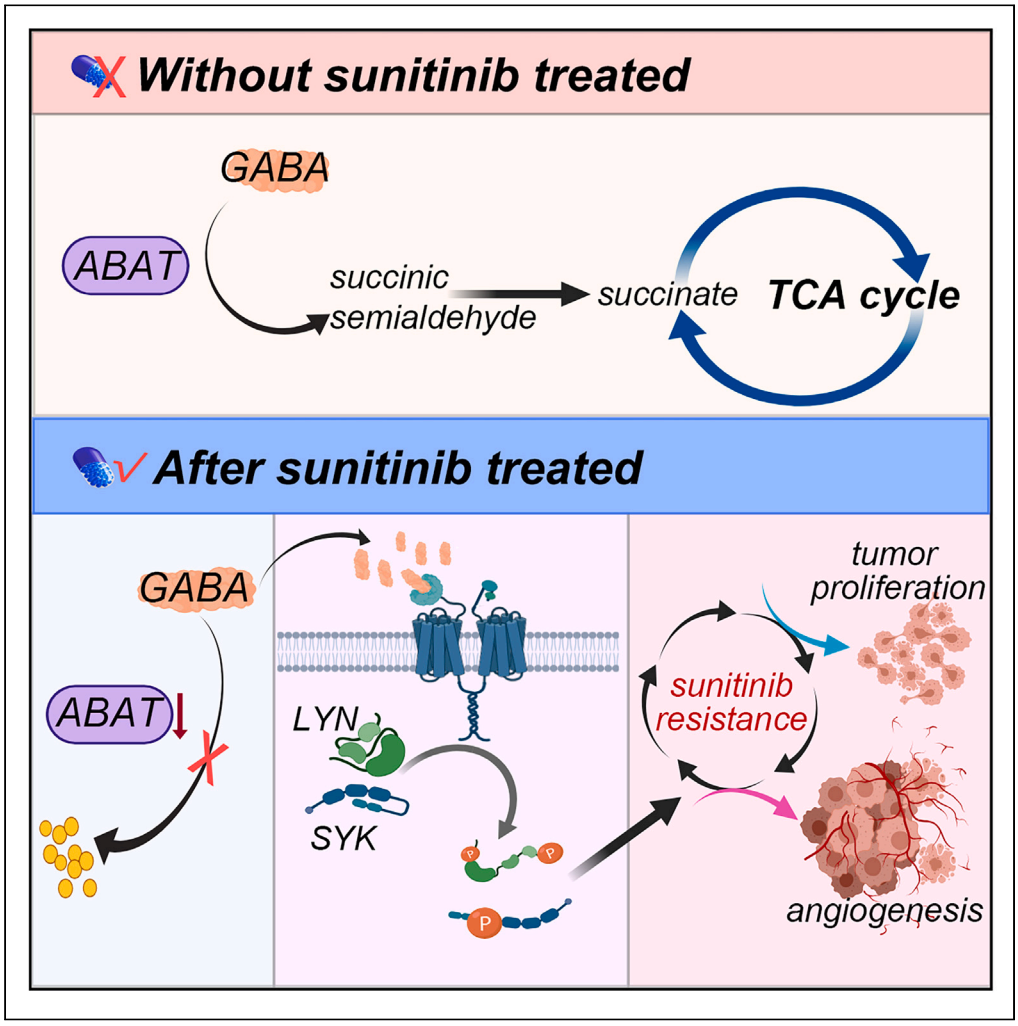

Qian Zhang, Lei Ding, Ye Yan, ..., Pengfei Shao, Chao Liang, Jie Li

spf032@hotmail.com (P.S.)
lc_machine@163.com (C.L.)
drc_lijie@126.com (J.L.)

Highlights

ABAT downregulation disrupts GABA metabolism, causing its accumulation in cells

GABA transactivates tyrosine kinases LYN and SYK through its receptor GABA-B

Activated LYN and SYK promote sunitinib resistance in ccRCC cells

LYN is key to blocking sunitinib resistance from GABA metabolic dysregulation

Zhang et al., iScience 27, 110415
July 19, 2024
https://doi.org/10.1016/j.isci.2024.110415

iScience

CellPress
OPEN ACCESS

Article

Decoding sunitinib resistance in ccRCC: Metabolic-reprogramming-induced ABAT and GABAergic system shifts

Qian Zhang,[1,2,4] Lei Ding,[1,4] Ye Yan,[3,4] Qidi Zhai,[1,4] Zhisheng Guo,[1] Yibo Li,[1] Zhentao Tang,[1] Pan Zang,[1] Chenbo Ni,[1] Shaobo Zhang,[1] Jian Qian,[1] Peng Han,[1] Pu Li,[1] Pengfei Shao,[1,*] Chao Liang,[1,*] and Jie Li[1,5,*]

SUMMARY

Sunitinib, a primary treatment for clear cell renal cell carcinoma (ccRCC), frequently encounters the challenge of resistance development. Metabolic reprogramming, a characteristic change in ccRCC, is likely linked to this resistance. Our research revealed a notable decrease in the expression of the key metabolic gene ABAT in ccRCC, which contributed to diminished sensitivity to sunitinib. Downregulation of ABAT led to an increase in the intracellular level of gamma-aminobutyric acid (GABA), triggering abnormal activation of the G-protein-coupled receptor GABA-B. This activation resulted in increased transactivation of the tyrosine kinase receptors SYK and LYN, thereby reducing the antitumor and antiangiogenic properties of sunitinib. However, the application of SYK and LYN inhibitors successfully inhibited this effect. The transactivation of SYK and LYN caused resistance to the antiangiogenic effects of sunitinib through the upregulation of PGF protein levels. Furthermore, the combined application of an LYN inhibitor with sunitinib has been shown to enhance therapeutic efficacy.

INTRODUCTION

Renal cell carcinoma (RCC), originating from the renal parenchyma,[1,2] is one of the most common tumors in the urinary system. Among the different subtypes of RCC, clear cell renal cell carcinoma (ccRCC) accounts for 75%–80% of all RCC cases and is a leading cause of mortality associated with RCC.[1,3] The majority of ccRCC patients (50%–75%) exhibit inactivation of the *Von Hippel–Lindau* (*VHL*) gene.[4,5] The product of the *VHL* gene, pVHL, plays a critical role in downregulating the expression of the *hypoxia-inducible factor 1* (*HIF1*) gene. Loss of pVHL leads to the accumulation of HIF1, which in turn increases the transcription of HIF1 target genes, such as *vascular endothelial growth factor* (*VEGF*) and *platelet-derived growth factor* (*PDGF*), ultimately promoting angiogenesis. Consequently, various antiangiogenic drugs, including sunitinib, pazopanib, sorafenib, and axitinib, have been developed for the treatment of RCC. Among these options, sunitinib is currently considered the frontline therapeutic option for RCC.[1]

Sunitinib is an orally administered tyrosine kinase inhibitor that primarily targets tumor angiogenesis by blocking key genes involved in the pathogenesis of ccRCC, specifically VEGFR and PDGFR. However, the initial response rate to sunitinib is typically approximately 30%–40%.[6–8] Consequently, disease progression often occurs within 6–15 months,[9] suggesting the presence of primary and/or secondary resistance mechanisms. The established mechanisms of sunitinib resistance include upregulation of proangiogenic signaling pathways, resistance mediated by the tumor microenvironment, increased tumor invasiveness and metastasis, activation of alternative pathways, and inadequate inhibition of the target.

The primary mechanism of action of sunitinib is to induce tumor hypoxia and necrosis, thereby reducing tumor burden.[10] However, tumors larger than 1 mm^3 often contain hypoxic regions, and tumor hypoxia is associated with increased invasion and metastasis and decreased patient survival rate. RCC adapts to hypoxic environments by undergoing metabolic reprogramming, which may contribute to resistance against targeted antiangiogenic therapy.

Understanding the metabolic changes that occur in RCC as it adapts to hypoxic environments is crucial for addressing tumor growth under adverse conditions. Therefore, this study aimed to investigate the mechanisms of sunitinib resistance from the perspective of metabolic alterations.

[1]Department of Urology, The First Affiliated Hospital of Nanjing Medical University, Nanjing, China
[2]Department of Urology, Jiangsu Taizhou People's Hospital, Taizhou 225300, China
[3]Department of Urology, Peking University Third Hospital, Haidian District, Beijing, People's Republic of China
[4]These authors contributed equally
[5]Lead contact
*Correspondence: spf032@hotmail.com (P.S.), lc_machine@163.com (C.L.), drc_lijie@126.com (J.L.)
https://doi.org/10.1016/j.isci.2024.110415

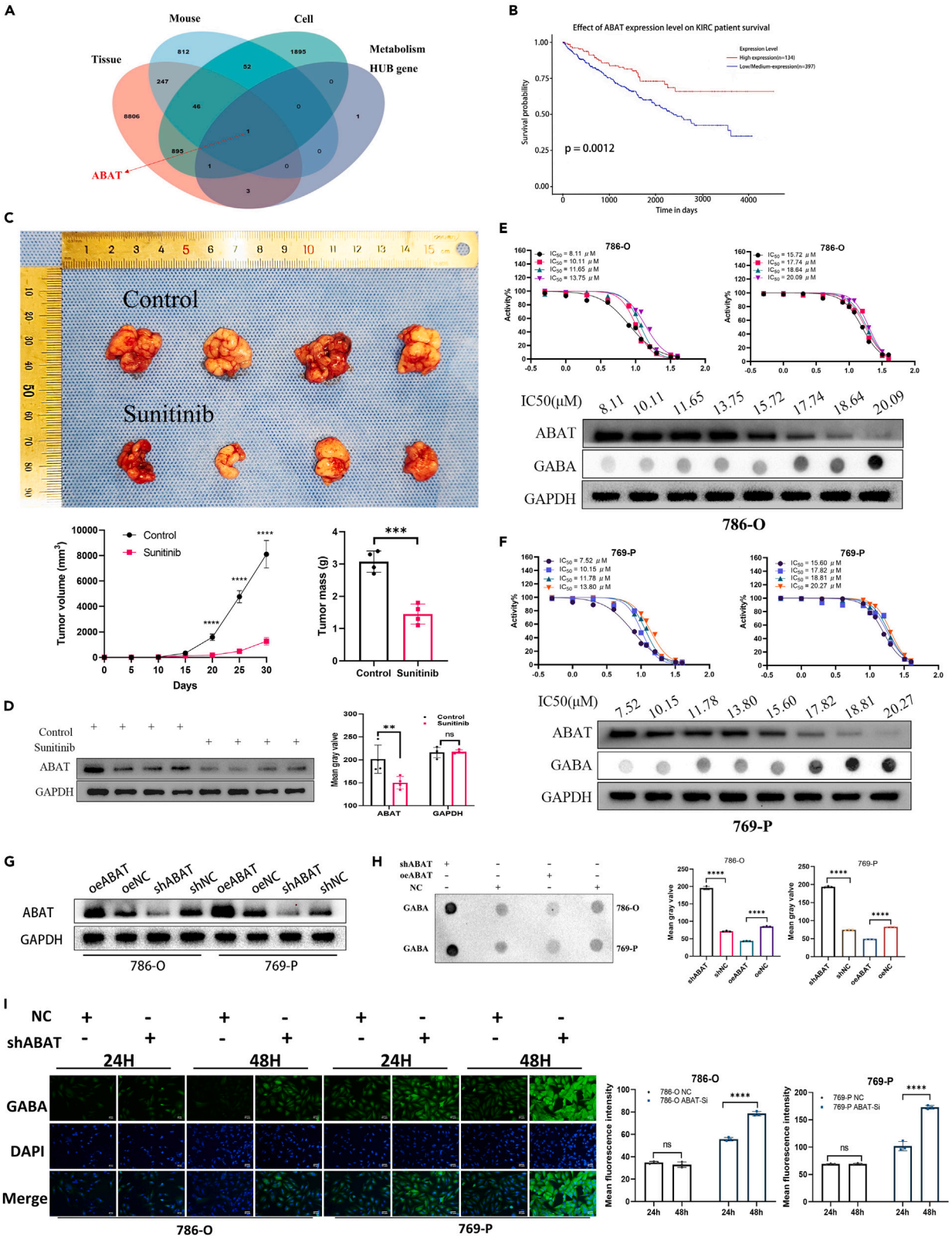
A
Mouse
Cell
Tissue
Metabolism
HUB gene
812
1895
52
247
0
46
0
1
8806
1
895
0
1
0
3
ABAT
B
Effect of ABAT expression level on KIRC patient survival
Expression Level
High expression(n=134)
Low/Medium-expression(n=397)
Survival probability
p = 0.0012
Time in days
C
Control
Sunitinib
Control
Sunitinib
Tumor volume (mm3)
Days
Tumor mass (g)
Control
Sunitinib
D
Control
Sunitinib
ABAT
GAPDH
Mean gray valve
ABAT
GAPDH
E
786-O
IC50 = 8.11 μM
IC50 = 10.11 μM
IC50 = 11.65 μM
IC50 = 13.75 μM
IC50 = 15.72 μM
IC50 = 17.74 μM
IC50 = 18.64 μM
IC50 = 20.09 μM
Activity%
IC50(μM)
8.11
10.11
11.65
13.75
15.72
17.74
18.64
20.09
ABAT
GABA
GAPDH
786-O
F
769-P
IC50 = 7.52 μM
IC50 = 10.15 μM
IC50 = 11.78 μM
IC50 = 13.80 μM
IC50 = 15.60 μM
IC50 = 17.82 μM
IC50 = 18.81 μM
IC50 = 20.27 μM
Activity%
IC50(μM)
7.52
10.15
11.78
13.80
15.60
17.82
18.81
20.27
ABAT
GABA
GAPDH
769-P
G
oeABAT
oeNC
shABAT
shNC
ABAT
GAPDH
786-O
769-P
H
shABAT
ocABAT
NC
GABA
GABA
786-O
769-P
Mean gray valve
I
NC
shABAT
24H
48H
24H
48H
GABA
DAPI
Merge
786-O
769-P
786-O
786-O NC
786-O ABAT-Si
Mean fluorescence intensity
769-P
769-P NC
769-P ABAT-Si
Mean fluorescence intensity

Figure 1. ABAT downregulated and elevated GABA levels in sunitinib-resistant ccRCC

(A) Screen metabolism-related sunitinib-resistant differentially expressed genes.

(B) Effect of ABAT expression level on ccRCC patient survival (high expression, $n = 134$; low/medium expression, $n = 397$).

(C) Treatments with control (vegetable oil) or sunitinib (40 mg/kg in vegetable oil) were administered separately to heterograft tumors (769-P cell line), and tumor growth was recorded ($n = 4$/group).

(D) Western blotting was used to detect changes in ABAT protein levels after treatment with the control or sunitinib ($n = 4$/group).

(E and F) Along with the increase in sunitinib IC50 values, the protein level changes in ABAT (the 786-O and 769-P cell lines) (see Figures S3I and S3J for statistical graphs of ABAT and GABA).

(G) Western blot showing the ABAT protein levels in 786-O ABAToe, 769-P ABAToe, 786-O ABATsh, and 769-P ABATsh cells (see Figure S3K for statistical graph). Representative blots ($n = 3$ experiments) are shown. x axis, log10 drug concentrations. y axis, Activity%, the percentage of cellular or biological activity in the drug-treated group relative to the control group.

(H) Dot blot showing GABA levels in 786-O ABAToe, 769-P ABAToe, 786-O ABATsh, and 769-P ABATsh cells. Representative blots ($n = 3$ experiments) are shown.

(I) Changes in the intracellular GABA concentration over time after ABAT regulation (NC vs. shABAT, $n = 3$ technical replicates per condition). The data are presented as the means ± SEMs. Groups were compared using two-way ANOVA with Sidak's multiple comparisons test, one-way ANOVA with Tukey's multiple comparisons test, two-way ANOVA with Tukey's multiple comparisons test, or unpaired t test where appropriate. Each spot represents one subject. NC, negative control; ns, not significant; $^{**}p < 0.01$, $^{***}p < 0.0001$, $^{****}p < 0.0001$. See also Figure S3.

RESULTS

The key metabolic gene ABAT was downregulated in sunitinib-resistant ccRCC

To identify potential drivers of sunitinib resistance, we initially analyzed gene expression data from human RCC samples treated with sunitinib as neoadjuvant therapy (GEO: GSE65615) and from patients treated with surgery alone (GEO: GSE68629), both of which were obtained from the Gene Expression Omnibus (GEO) database. After removing batch effects (Figures S1A and S1B), we combined these datasets into a matrix and analyzed the major gene changes before and after sunitinib treatment, resulting in the identification of 9,998 differentially expressed genes (DEGs) (Figure S2A). Additionally, we examined the GEO: GSE76068 dataset from the GEO database, which contains gene expression data from a xenograft model of RCC in mice during sunitinib resistance, and revealed 1,158 DEGs (Figure S2B). Furthermore, we identified 2,890 DEGs (Figure S2C) in cell line samples of sunitinib-resistant RCC (GEO: GSE64052). By overlapping these three sets of DEGs, we identified 47 common DEGs (Figure S2D). Heatmap analysis revealed elevated levels of HIF1A in the resistant group (Figure S2E), indicating a potential link between sunitinib-induced tumor hypoxia and active adaptation to the hypoxic environment.[11–14]

The activation of HIF1A to regulate metabolic pathways and stimulate angiogenesis is a primary mechanism by which tumors adapt to hypoxic environments. Previously, we identified six crucial metabolic genes (ABAT, ALDH6A1, CHDH, EPHX2, ETNK2, and FBP1) closely associated with the prognosis of ccRCC.[15] To further identify metabolism-related genes among the 47-intersecting resistant DEGs, we intersected them with the six key metabolic genes, leading to the identification of the key gene gamma-aminobutyrate aminotransferase (*ABAT*) (Figure 1A). Initial examination of ABAT in ccRCC using the UALCAN database revealed significant decreases in both the transcript and protein levels (Figures S3A–S3F), which were strongly correlated with poor patient prognosis (Figure 1B). A similar association between decreased ABAT levels and adverse outcomes was also observed in liver, kidney, and breast cancer patients.[16–21]

Using the Human Protein Atlas (HPA) database (Figures S3G–S3H), which contains proteomic data from normal and tumor tissues, we compared the protein expression levels of ABAT in normal kidney tissues and RCC tissues via two antibody stains, HPA041528 and HPA041690. The results demonstrated a significant reduction in ABAT protein levels in RCC tissues.

To observe the changes in ABAT during the development of sunitinib resistance, we established sunitinib-resistant strains (786-O and 769-P) (Figure S3L). During the construction of the sunitinib-resistant strains, we recorded the half-maximal inhibitory concentrations (IC50) of sunitinib and the corresponding ABAT protein levels (Figures 1E and 1F). The results revealed a decrease in ABAT protein levels as the sunitinib IC50 increased (Figures S3I and S3J). Additionally, 769-P cells were transplanted subcutaneously into nude mice, which were treated with either oral vegetable oil or sunitinib after the tumor was stabilized for 5 days (Figure 1C). ABAT levels were measured after 4 weeks (Figure 1D), and the sunitinib-treated group exhibited lower ABAT levels in the xenograft tumors than did the control group (Figure 1D). In summary, our findings indicate that sunitinib treatment reduces the expression of the metabolic gene ABAT, and during the progression of sunitinib resistance, the protein expression of ABAT gradually decreases.

Reduced ABAT expression elevates GABA levels in ccRCC patients

Gamma-aminobutyric acid (GABA), a neurotransmitter present not only in the nervous system but also in nonneuronal tissues, is regulated by the enzyme ABAT.[22,23] ABAT ensures the proper metabolism of GABA, thereby maintaining its levels within cells. In our study, we observed a gradual decrease in ABAT protein levels, accompanied by an increase in GABA levels, as sunitinib resistance developed in the 786-O and 769-P cell lines. These findings suggest that reduced ABAT protein levels hinder the timely degradation of GABA, leading to its accumulation within cells.

To investigate the effect of decreased ABAT protein levels on intracellular GABA levels, we manipulated ABAT expression in cell lines through overexpression (786-O ABAToe and 769-P ABAToe) and knockdown (786-O ABATsh and 769-P ABATsh) techniques (Figures 1G and S3K). Modulating ABAT protein levels allowed us to assess intracellular GABA levels, confirming the significant influence of ABAT on GABA regulation (Figure 1H). Additionally, we monitored the accumulation of intracellular GABA in the ABAT-knockdown groups at 24 and 48 h post-knockdown. The fluorescence intensity of intracellular GABA gradually increased over time in the ABAT knockdown group

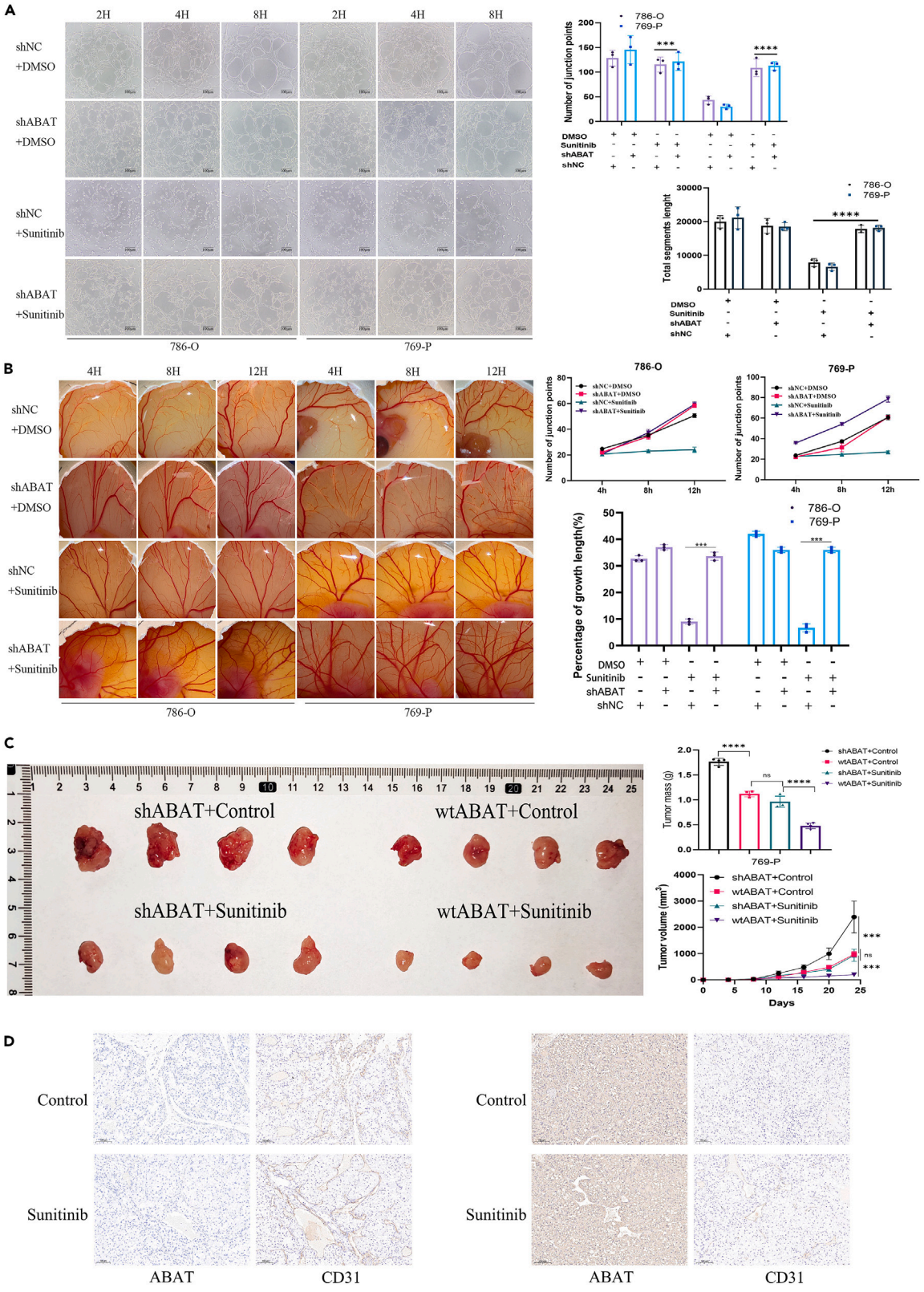
A
2H
4H
8H
2H
4H
8H
shNC
+DMSO
shABAT
+DMSO
shNC
+Sunitinib
shABAT
+Sunitinib
786-O
769-P
Number of junction points
786-O
769-P
***
****
DMSO
Sunitinib
shABAT
shNC
Total segments lenght
786-O
769-P
****
DMSO
Sunitinib
shABAT
shNC
B
4H
8H
12H
4H
8H
12H
shNC
+DMSO
shABAT
+DMSO
shNC
+Sunitinib
shABAT
+Sunitinib
786-O
769-P
786-O
769-P
Number of junction points
shNC+DMSO
shABAT+DMSO
shNC+Sunitinib
shABAT+Sunitinib
4h
8h
12h
Percentage of growth length(%)
786-O
769-P
***
DMSO
Sunitinib
shABAT
shNC
C
shABAT+Control
wtABAT+Control
shABAT+Sunitinib
wtABAT+Sunitinib
Tumor mass (g)
****
ns
****
769-P
Tumor volume (mm³)
Days
***
ns
***
D
Control
Sunitinib
ABAT
CD31
Control
Sunitinib
ABAT
CD31

Figure 2. A reduction in ABAT diminishes sunitinib sensitivity and its antiangiogenic effects

(A) Tube formation assays using HUVECs cultured in conditioned medium from ccRCC cells (shABAT vs. shNC, treated with DMSO or sunitinib for 24 h).

(B) Chick embryo chorioallantoic membrane (CAM) assays with conditioned medium from ccRCC cells (shABAT vs. shNC, treated with DMSO or sunitinib, 24 h).

(C) Treatments with control (vegetable oil) or sunitinib (40 mg/kg in vegetable oil) were administered separately to heterograft tumors (769-P ABATsh and 769-P ABATwt cells), and tumor growth was recorded (n = 4/group).

(D) The vascular density of the heterograft tumors (769-P ABATsh vs. 769-P ABATwt, n = 4/group). The data are presented as the means ± SEMs. Groups were compared using one-way ANOVA with Tukey's multiple comparisons test, two-way ANOVA with Tukey's multiple comparisons test, or unpaired t test where appropriate. Each spot represents one subject. NC, negative control; ns, not significant; ***$p < 0.0001$, ****$p < 0.0001$.

(Figure 1I). These findings demonstrated that the decrease in ABAT levels during sunitinib resistance progression in ccRCC results in the accumulation of intracellular GABA (Figure S3M).

Altered ABAT expression influences the antiangiogenic effects of sunitinib

CcRCC is a highly vascularized tumor, and sunitinib is a commonly used therapeutic agent for this disease. As an orally administered tyrosine kinase inhibitor, sunitinib has both antitumor growth and antiangiogenic effects. However, the initial response rate of these materials is less than 50%, and resistance often develops over time. To explore the influence of decreased ABAT levels, a key metabolic gene, on the antiangiogenic effects of sunitinib, we manipulated ABAT expression in two ccRCC cell lines and conducted subsequent experiments.

The ABAT-knockdown cells (cell lines 786-O ABATsh and 769-P ABATsh) and the control cells (cell lines 786-O ABATwt and 769-P ABATwt) were initially treated with either dimethyl sulfoxide (DMSO) or sunitinib for 24 h. The cell culture medium was subsequently added to human umbilical vein endothelial cells (HUVECs), and the formation of vascular tubes was recorded at 2 h, 4 h, and 8 h. The results showed that DMSO in the control group had no significant effect on HUVEC tube formation, whereas sunitinib markedly inhibited both the number and length of tubes formed by HUVECs (Figure 2A). Interestingly, the ABAT-knockdown group displayed resistance to the inhibitory effects of sunitinib on HUVEC tube formation.

Furthermore, DMSO tumor-conditioned medium (TCM) and sunitinib TCM were administered to the chorioallantoic membrane (CAM) of 5-day-old chick embryos, and changes in blood vessel length and branching points were recorded at 4 h, 8 h, and 12 h. The results demonstrated that chick embryos cultured in the cell culture media of 786-O ABATwt and 769-P ABATwt cells treated with sunitinib did not exhibit significant vascular changes. In contrast, embryos exposed to the cell culture media of 786-O ABATsh and 769-P ABATsh cells treated with sunitinib exhibited marked increases in blood vessel branching and length (Figure 2B). These findings suggested that decreased ABAT levels influence the antiangiogenic efficacy of sunitinib during the progression of sunitinib resistance in ccRCC.

We implanted 769-P ABATsh and 769-P ABATwt cells subcutaneously into nude mice. After stable tumor formation for 4 days, the mice were treated with either vegetable oil or sunitinib via oral administration for 5 days a week. Tumor diameters were then measured every 4 days. We observed that sunitinib had a less effective inhibitory effect on 769-P ABATsh tumors than on control tumors (Figure 2C). After 4 weeks, the tumors were harvested for immunohistochemical examination, which revealed greater vascular density in the 769-P ABATsh tumors than in the 769-P ABATwt tumors (Figure 2D).

GABA-B receptor aberrant activation impairs sensitivity to sunitinib therapy

We observed a decrease in ABAT expression in RCC tumor tissues compared to normal tissues. Treatment with sunitinib further reduced ABAT expression, leading to the accumulation of GABA due to impaired timely degradation. GABA exerts its effects through GABA-A and GABA-B receptors, with GABA-A receptors being ionotropic and coupled to chloride ion channels, whereas GABA-B receptors are metabotropic and belong to the family of G-protein-coupled receptors (GPCRs), which play a crucial role in cellular signal transduction involving various tyrosine kinases.[24–26]

The accumulation of GABA resulting from reduced ABAT levels may activate GABA-B receptors, influencing the therapeutic effects of the tyrosine kinase inhibitor sunitinib. Therefore, we separately assessed the IC50 of sunitinib in untreated cells, ABAT-knockdown cells, cells treated with baclofen (a GABAB receptor agonist), and cells treated with phaclofen (a GABAB receptor antagonist) (Figure 3A). The experimental results showed a slight decrease in the IC50 in cells treated with phaclofen compared to that in untreated cells. In contrast, ABAT-knockdown cells and baclofen-treated cells exhibited significant increases in the IC50 compared to those of the control group. Activation of GABA-B receptors and decreased ABAT levels both affected the drug sensitivity of sunitinib.

Early studies indicated a close correlation between GPCRs and cell proliferation, with sunitinib exerting direct toxic effects on tumor cells.[27] To explore the effects of ABAT alterations and GABAB receptor regulation on cell proliferation under sunitinib treatment, we utilized EdU staining to quantify proliferating cells under different treatment conditions (Figures 3B and 3C). Compared to those in the control group, the number of proliferating cells in both the ABAT-overexpressing group and the phaclofen-treated group was significantly lower after sunitinib treatment, whereas sunitinib treatment did not significantly decrease the number of proliferating cells in the ABAT-knockdown group or the baclofen-treated group.

We further assessed the effect of regulating GABA-B receptors and ABAT knockdown on the inhibitory effects of sunitinib on angiogenesis. Initially, ABATwt cells were divided into three groups and subjected to individual treatments with control, baclofen, or phaclofen for 30 min. Subsequently, these cells were coincubated with ABATsh cells and exposed to sunitinib for 24 h. Tumor cell culture medium from each of the four groups was then added to HUVECs, and vascular formation was recorded at 2 h, 4 h, and 8 h (Figure 3D). Our findings revealed

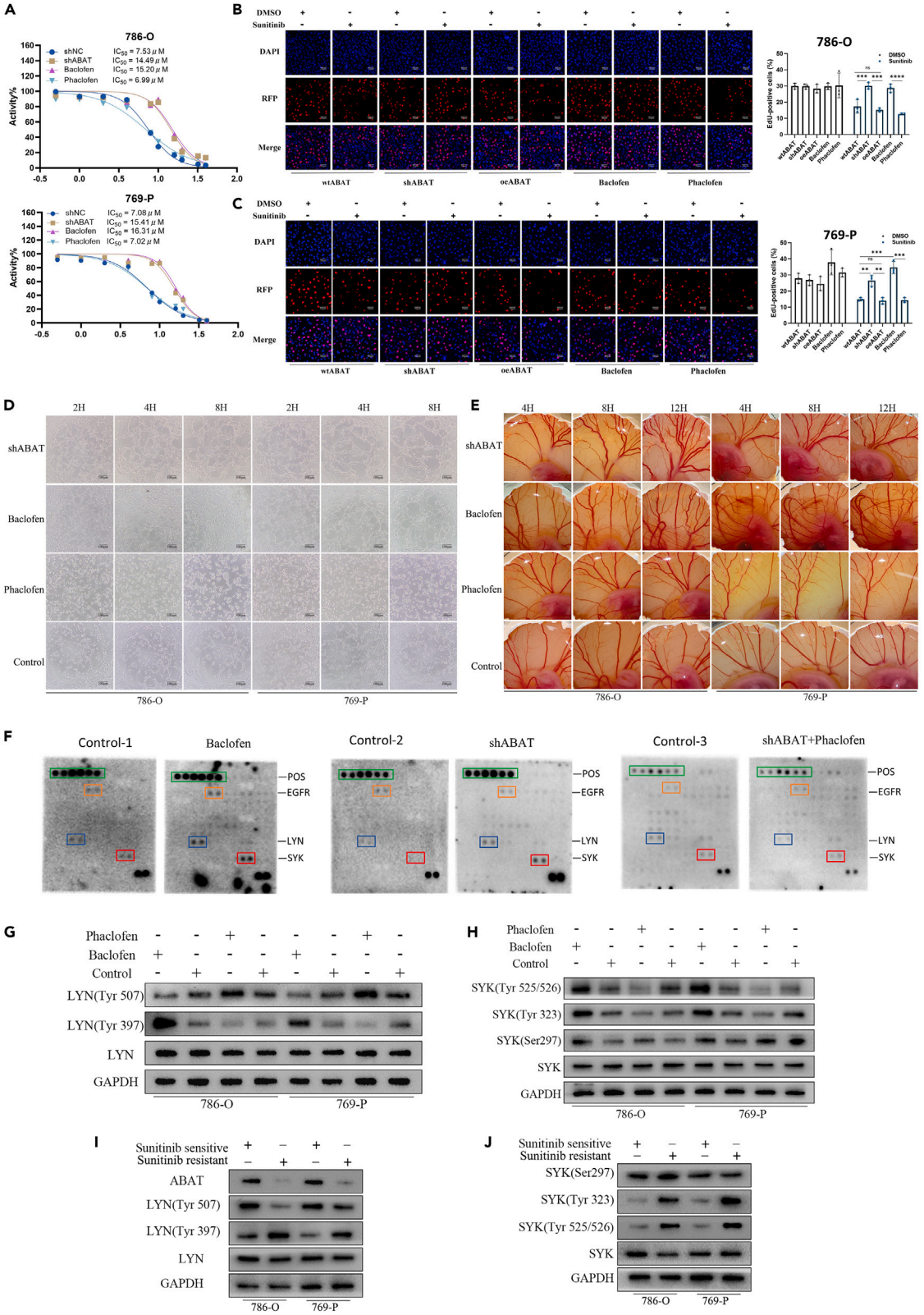
A
786-O
shNC IC50 = 7.53 μM
shABAT IC50 = 14.49 μM
Baclofen IC50 = 15.20 μM
Phaclofen IC50 = 6.99 μM
Activity%
769-P
shNC IC50 = 7.08 μM
shABAT IC50 = 15.41 μM
Baclofen IC50 = 16.31 μM
Phaclofen IC50 = 7.02 μM
B
DMSO
Sunitinib
DAPI
RFP
Merge
wtABAT
shABAT
oeABAT
Baclofen
Phaclofen
786-O
EdU-positive cells (%)
C
769-P
D
2H
4H
8H
shABAT
Baclofen
Phaclofen
Control
786-O
769-P
E
12H
F
Control-1
Baclofen
Control-2
shABAT
Control-3
shABAT+Phaclofen
POS
EGFR
LYN
SYK
G
LYN(Tyr 507)
LYN(Tyr 397)
LYN
GAPDH
H
SYK(Tyr 525/526)
SYK(Tyr 323)
SYK(Ser297)
I
Sunitinib sensitive
Sunitinib resistant
ABAT
J

Figure 3. Downregulation of ABAT increases the phosphorylation of SYK and LYN through activation of GABA-B receptors

(A) Effect of ABAT (NC vs. shABAT) and GABA-B receptors (baclofen or phaclofen) on the IC50 of sunitinib (n = 3 technical replicates per condition). x axis, log10 drug concentrations. y axis, Activity%, the percentage of cellular or biological activity in the drug-treated group relative to the control group.

(B and C) The impact of regulating ABAT (NC vs. shABAT vs. oABAT) and GABA-B receptors (baclofen or phaclofen) on the antitumor efficacy of sunitinib.

(D) Tube formation assays of HUVECs cultured in conditioned medium from ccRCC cells in four groups: control, shABAT, baclofen (100 μM), and phaclofen (100 μM) (treated with Sunitinib for 24 h) (see Figures S4A and S4B for statistical graph).

(E) Chick embryo chorioallantoic membrane (CAM) assays with conditioned medium from ccRCC cells in four groups: control, shABAT, baclofen (100 μM), and phaclofen (100 μM) (treated with sunitinib for 24 h) (see Figures S4C and S4E for statistical graph).

(F) Microarray analysis of the regulatory effects of ABAT and GABA-B on the phosphorylation levels of various tyrosine kinases (see Figure S4F for statistical graph) in 769-P cells.

(G) Western blot of LYN, LYN (Tyr 507), and LYN (Tyr 397) in ccRCC cells (786-O and 769-P) treated with the control (phosphate-buffered saline, PBS, pH 7.6), baclofen (100 μM), or phaclofen (100 μM) for 30 min (see Figure S4G for statistical graph). The data represent one of two independent experiments.

(H) Western blot of SYK, SYK (Tyr 297), SYK (Tyr 323), and SYK (Tyr 525/526) in ccRCC cells (786-O and 769-P) treated with the control (phosphate-buffered saline, PBS, pH 7.6), baclofen (100 μM), or phaclofen (100 μM) for 30 min (see Figure S4H for statistical graph). Representative blots (n = 3 experiments).

(I and J) Western blot of ABAT, LYN, SYK, LYN (Tyr 507), LYN (Tyr 397), SYK (Tyr 297), SYK (Tyr 323), and SYK (Tyr 525/526) in sunitinib-sensitive (786-O S and 769-P S) and -resistant (786-O R and 769-P R) ccRCC cells (see Figures S4I and S4J for statistical graph). The data represent one of two independent experiments. The data are presented as the means ± SEMs. Groups were compared using two-way ANOVA with Tukey's multiple comparisons test, two-way ANOVA with Dunnett's multiple comparisons test, or unpaired t test where appropriate. Each spot represents one subject. POS, positive control spot; ns, not significant; $^{**}p < 0.01$, $^{***}p < 0.0001$, $^{****}p < 0.0001$. See also Figure S4.

a significantly enhanced tube-forming ability in the ABAT knockdown group and the baclofen-treated group compared to the control group and the phaclofen-treated group (Figures S4A and S4B). Moreover, experiments conducted on the CAM of chick embryos (Figure 3E) showed that the ABAT knockdown group and baclofen-treated group exhibited markedly greater blood vessel length and branching points than did the control group and the phaclofen-treated group (Figures S4C–S4E). These results imply that the decrease in sunitinib drug sensitivity and antiangiogenic function due to the ABAT reduction may be attributed to the intracellular accumulation of GABA, which thereby activates GABA-B receptors.

Aberrant GABA-B activation increases the phosphorylation levels of SYK and LYN

GPCRs are closely related to tyrosine kinases. Reported examples demonstrate the ability of GPCRs to sequester and activate tyrosine kinase receptors even in the absence of the corresponding ligands, a phenomenon known as "transactivation."[28,29] GABA-B receptors, characterized as seven transmembrane GPCRs, play a role in influencing the antitumor and antiangiogenic effects of sunitinib, potentially through tyrosine kinase receptor transactivation. To investigate the activated tyrosine kinase receptors, we employed a tyrosine kinase receptor microarray (Figures 3F and S4F). Compared to those in the control group, the phosphorylation levels of EGFR in the baclofen-treated group were elevated. Furthermore, both baclofen treatment and ABAT knockdown led to increased phosphorylation levels of LYN and SYK. However, in the ABAT knockdown group treated with phaclofen, the phosphorylation and activation of LYN and SYK were inhibited. Therefore, decreased ABAT levels activating GABA-B receptors result in heightened phosphorylation levels of SYK and LYN.

Analysis of the database data revealed that the protein levels of SYK and LYN were significantly greater in RCC tissues than in normal renal tissues (Figures S5A–S5C). Further investigation of the modulation of GABA-B receptors indicated that changes in the protein levels of LYN and SYK were not significant, but activation of GABA-B receptors resulted in an increase in the phosphorylation of SYK at Tyr323 and Tyr525/526 (Figures 3H and S4H) or in the phosphorylation of LYN at Tyr397 (Figures 3G and S4G). Further analysis, an increase in the phosphorylation of the Tyr323 and Tyr525/526 sites of SYK (Figure 3J), as well as the Tyr397 site of LYN (Figure 3I), was observed in sunitinib-resistant cell lines (Figures S4I and S4J). Notably, phosphorylation at Tyr507 inhibits the function of LYN, whereas dephosphorylation at Tyr507 activates the functional domain, leading to phosphorylation at Tyr397.[30,31] To understand the relationships between ABAT alterations and LYN and SYK expression, ABAT was knocked down, and measurements were taken at 0 h, 12 h, 24 h, 36 h, 48 h, and 72 h (Figures 4A and 4B). As the ABAT protein concentration decreased, the phosphorylation of SYK at Tyr323 and Tyr525/526, as well as that of LYN at Tyr397, gradually increased, whereas the protein levels of LYN and SYK did not significantly change (Figures S6A and S6B).

Elevated phosphorylation levels of SYK and LYN impact the efficacy of sunitinib treatment

We observed a decrease in ABAT, resulting in the activation of GABA-B receptors and the upregulation of SYK and LYN phosphorylation. To confirm the impact of changes in SYK and LYN phosphorylation on sunitinib resistance, we established the following plasmid-based stable mutant cell lines: 786-O $SYK^{Y323/525E}$ and 769-P $SYK^{Y323/525E}$ for stable SYK phosphorylation (Figures 4C and S6E); 786-O $SYK^{Y323/525F}$ and 769-P $SYK^{Y323/525F}$ for stable SYK dephosphorylation (Figures 4D and S6F); 786-O LYN^{Y397E} and 769-P LYN^{Y397E} for stable LYN phosphorylation (Figures 4E and S6C); and 786-O LYN^{Y397F} and 769-P LYN^{Y397F} for stable LYN dephosphorylation (Figures 4F and S6D). These cell lines allowed us to control the phosphorylation status of SYK and LYN at the cellular level. We found that, compared to those in the control and dephosphorylation groups, the activation of LYN and SYK phosphorylation significantly increased the IC50 of sunitinib (Figure 4G). Additionally, under sunitinib treatment, the number of proliferative cells in the LYN and SYK phosphorylation groups was greater than that in the control and dephosphorylation groups (Figures 4H and 4I), indicating that the activation of LYN and SYK phosphorylation reduced the antitumor effect of sunitinib.

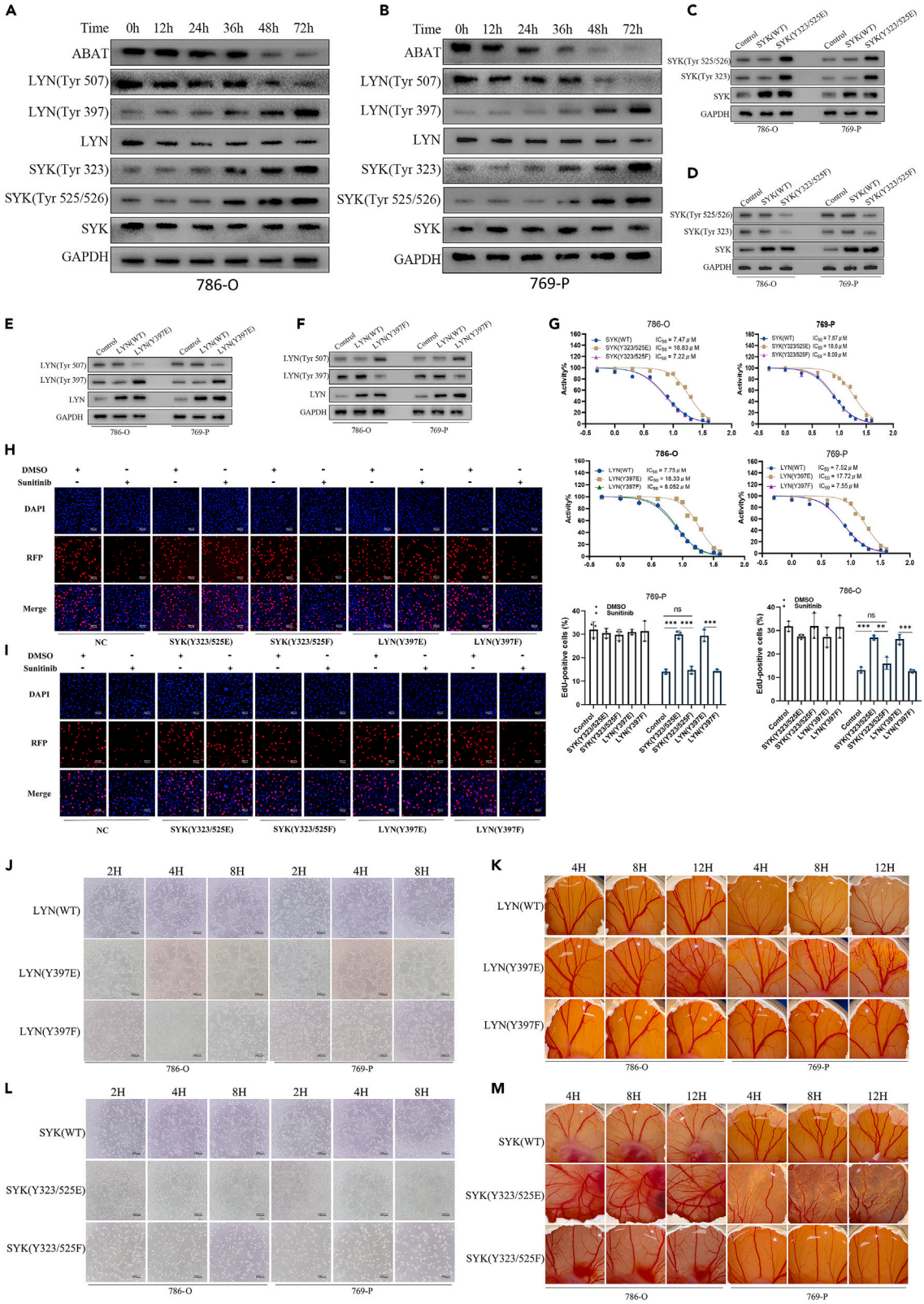
A
Time 0h 12h 24h 36h 48h 72h
ABAT
LYN(Tyr 507)
LYN(Tyr 397)
LYN
SYK(Tyr 323)
SYK(Tyr 525/526)
SYK
GAPDH
786-O
B
Time 0h 12h 24h 36h 48h 72h
ABAT
LYN(Tyr 507)
LYN(Tyr 397)
LYN
SYK(Tyr 323)
SYK(Tyr 525/526)
SYK
GAPDH
769-P
C
Control
SYK(WT)
SYK(Y323/525E)
SYK(Tyr 525/526)
SYK(Tyr 323)
SYK
GAPDH
786-O
769-P
D
Control
SYK(WT)
SYK(Y323/525F)
SYK(Tyr 525/526)
SYK(Tyr 323)
SYK
GAPDH
786-O
769-P
E
Control
LYN(WT)
LYN(Y397E)
LYN(Tyr 507)
LYN(Tyr 397)
LYN
GAPDH
786-O
769-P
F
Control
LYN(WT)
LYN(Y397F)
LYN(Tyr 507)
LYN(Tyr 397)
LYN
GAPDH
786-O
769-P
G
786-O
SYK(WT) IC50 = 7.47 μM
SYK(Y323/525E) IC50 = 16.83 μM
SYK(Y323/525F) IC50 = 7.22 μM
769-P
SYK(WT) IC50 = 7.87 μM
SYK(Y323/525E) IC50 = 18.6 μM
SYK(Y323/525F) IC50 = 8.09 μM
Activity%
786-O
LYN(WT) IC50 = 7.75 μM
LYN(Y397E) IC50 = 18.33 μM
LYN(Y397F) IC50 = 8.052 μM
769-P
LYN(WT) IC50 = 7.52 μM
LYN(Y397E) IC50 = 17.72 μM
LYN(Y397F) IC50 = 7.55 μM
Activity%
769-P
DMSO
Sunitinib
EdU-positive cells (%)
ns
786-O
DMSO
Sunitinib
EdU-positive cells (%)
ns
H
DMSO
Sunitinib
DAPI
RFP
Merge
NC
SYK(Y323/525E)
SYK(Y323/525F)
LYN(Y397E)
LYN(Y397F)
I
DMSO
Sunitinib
DAPI
RFP
Merge
NC
SYK(Y323/525E)
SYK(Y323/525F)
LYN(Y397E)
LYN(Y397F)
J
2H 4H 8H 2H 4H 8H
LYN(WT)
LYN(Y397E)
LYN(Y397F)
786-O
769-P
K
4H 8H 12H 4H 8H 12H
LYN(WT)
LYN(Y397E)
LYN(Y397F)
786-O
769-P
L
2H 4H 8H 2H 4H 8H
SYK(WT)
SYK(Y323/525E)
SYK(Y323/525F)
786-O
769-P
M
4H 8H 12H 4H 8H 12H
SYK(WT)
SYK(Y323/525E)
SYK(Y323/525F)
786-O
769-P

Figure 4. Elevated phosphorylation levels of SYK and LYN impact the efficacy of sunitinib treatment

(A and B) Western blot of ABAT, LYN, SYK, LYN(Tyr 507), LYN(Tyr 397), SYK(Tyr 297), SYK(Tyr 323), and SYK(Tyr 525/526) in ccRCC cells (786-O and 769-P) with ABAT knockdown 0 h, 12 h, 24 h, 36 h, 48 h, and 72 h (see Figures S6A and S6B for statistical graph).

(C–F) Western blot analysis of SYK and LYN phosphorylation levels during stable SYK phosphorylation (786-O $SYK^{Y323/525E}$ and 769-P $SYK^{Y323/525E}$), stable SYK dephosphorylation (786-O $SYK^{Y323/525F}$ and 769-P $SYK^{Y323/525F}$), stable LYN phosphorylation (786-O LYN^{Y397E} and 769-P LYN^{Y397E}), and stable LYN dephosphorylation (786-O LYN^{Y397F} and 769-P LYN^{Y397F}) (see Figures S6C–C6F for statistical graph). Representative blots (n = 3 experiments).

(G) Dose-response curves and corresponding IC50 of sunitinib for 786-O $SYK^{Y323/525E}$, 769-P $SYK^{Y323/525E}$, 786-O $SYK^{Y323/525F}$, 769-P $SYK^{Y323/525F}$, 786-O LYN^{Y397E}, 769-P LYN^{Y397E}, 786-O LYN^{Y397F}, 769-P LYN^{Y397F}, 786-O SYK^{WT}, 769-P SYK^{WT}, 786-O LYN^{WT}, and 769-P LYN^{WT} after treatment for 24 h are shown. x axis, log10 drug concentrations. y axis, Activity%, the percentage of cellular or biological activity in the drug-treated group relative to the control group.

(H and I) Compared to those in the SYK and LYN dephosphorylation and control groups, more EdU-labeled cells in the SYK and LYN phosphorylation groups (treated with sunitinib) were observed. The data represent one of two independent experiments.

(J) Tube formation assays of HUVECs cultured in conditioned medium from ccRCC cells (786-O LYN^{Y397E}, 769-P LYN^{Y397E}, 786-O LYN^{Y397F}, 769-P LYN^{Y397F}, 786-O LYN^{WT}, and 769-P LYN^{WT} cells treated with DMSO or Sunitinib for 24 h) (see Figures S6G and S6H for statistical graph).

(K) Chick embryo chorioallantoic membrane (CAM) assays with conditioned medium from ccRCC cells (786-O LYN^{Y397E}, 769-P LYN^{Y397E}, 786-O LYN^{Y397F}, 769-P LYN^{Y397F}, 786-O LYN^{WT}, and 769-P LYN^{WT}) treated with DMSO or sunitinib for 24 h (see Figures S6I–S6K for statistical graph).

(L) Tube formation assays using HUVECs cultured in conditioned medium from ccRCC cells (786-O $SYK^{Y323/525E}$, 769-P $SYK^{Y323/525E}$, 786-O $SYK^{Y323/525F}$, 769-P $SYK^{Y323/525F}$, 786-O SYK^{WT}, and 769-P SYK^{WT}) treated with DMSO or sunitinib for 24 h (see Figures S6L and S6M for statistical graph).

(M) Chick embryo chorioallantoic membrane (CAM) assays with conditioned medium from ccRCC cells (786-O $SYK^{Y323/525E}$, 769-P $SYK^{Y323/525E}$, 786-O $SYK^{Y323/525F}$, 769-P $SYK^{Y323/525F}$, 786-O SYK^{WT}, and 769-P SYK^{WT} cells treated with DMSO or sunitinib for 24 h) (see Figures S6N–S6P for statistical graph). The data are presented as the means ± SEMs. Groups were compared using two-way ANOVA with Holm-Sidak multiple comparisons test, two-way ANOVA with Tukey's multiple comparisons test, or unpaired t test where appropriate. Each spot represents one subject. ns, not significant; ***$p < 0.0001$, ****$p < 0.0001$. See also Figure S6.

To validate the impact of LYN and SYK phosphorylation on sunitinib resistance during angiogenesis, we treated cells with LYN and SYK phosphorylation mutants with sunitinib for 24 h. Subsequently, we cultured HUVECs (Figures 4J and 4L) and chicken embryo CAMs (Figures 4K and 4M) in conditioned media separately and observed tube formation (Figures S6G, S6H, S6N, and S6P) and vascular changes in the CAM (Figures S6I–S6K and S6N–S6P). We found that HUVEC tube formation and length were significantly greater in the LYN and SYK phosphorylation mutation groups than in the wild-type and nonphosphorylation mutation groups. Moreover, the number of blood vessel branches and the growth rate of blood vessel length in the LYN and SYK phosphorylation mutation groups were greater than those in the wild-type and nonphosphorylation mutation groups, indicating that increased levels of LYN and SYK phosphorylation led to a reduction in the anti-angiogenic effect of sunitinib.

Inhibiting LYN or SYK enhances sunitinib efficacy against resistant ccRCC

To validate whether the activation of the tyrosine kinase receptors SYK and LYN is the primary factor responsible for ABAT-induced resistance to sunitinib, we conducted experiments to inhibit the phosphorylation of SYK and LYN in ABAT-knockdown cells (ABATsh LYN^{Y397F} and ABATsh $SYK^{Y323/525F}$) (Figures 5A, 5B, S7A, and S7B). A comparison of the LYN and SYK inhibitor results revealed that inhibiting SYK phosphorylation and utilizing SYK inhibitors, as well as inhibiting LYN phosphorylation and employing LYN inhibitors, led to a reduction in the increase in the IC50 of sunitinib caused by ABAT abnormalities (Figure 5C).

The inhibition of LYN or SYK phosphorylation or the combination of sunitinib with LYN or SYK inhibitors also enhanced the inhibitory effect of sunitinib on blood vessels. As shown in Figure 5, the groups in which LYN or SYK was inhibited or the groups in which sunitinib was combined with LYN or SYK inhibitors exhibited significantly reduced tube formation and blood vessel length in HUVECs (Figures 5D, S7C, and S7D), as well as a significant decrease in the number of blood vessel branches and the growth rate of blood vessels in the chicken embryo CAM (Figures 5E, S7E, and S7F). In cells with decreased ABAT levels, the combined use of LYN or SYK inhibitors enhanced the drug sensitivity of sunitinib, resulting in a decrease in cell proliferation (Figure 5F). Consequently, we discovered a close association between a decrease in ABAT and reduced sensitivity to sunitinib, which was linked to increased phosphorylation levels of LYN and SYK. After sunitinib treatment, cells with reduced ABAT activate the GABA-B receptor by activating GABA, leading to the activation of the tyrosine kinase receptors SYK and LYN, which counteract the antitumor and antiangiogenic effects of sunitinib.

To explore the potential mutation between SYK phosphorylation and LYN phosphorylation, we separately assessed the phosphorylation levels of LYN in cells with and without SYK phosphorylation regulation, as well as the phosphorylation levels of SYK in cells with and without LYN phosphorylation regulation. Our findings demonstrated that phosphorylation of LYN increases the phosphorylation level of SYK, whereas phosphorylation of SYK has no significant effect on the phosphorylation of LYN (Figures 5G, 5H, S7G, and S7H). We further subcutaneously implanted 769-P S and 769-P R cells into nude mice. After stable tumor formation for 4 days, the mice were treated with vegetable oil, sunitinib, R406, PD173952, or a combination of sunitinib and PD173952 or R406 via oral administration for 5 days a week. Tumor diameters were then measured every 5 days. We observed that combined treatment with sunitinib and PD173952 or R406 effectively reduced the sunitinib resistance (Figures 5I, S7I, and S7J).

Elevated phosphorylation levels of SYK and LYN activate the AKT and STAT pathways

To investigate the impact of elevated phosphorylation levels of SYK and LYN on gene expression in ccRCC, we sequenced samples from wild-type and stable SYK- and LYN-phosphorylated ccRCC cells (Figures 6A and 6B). By analyzing the genes that exhibited significant changes and

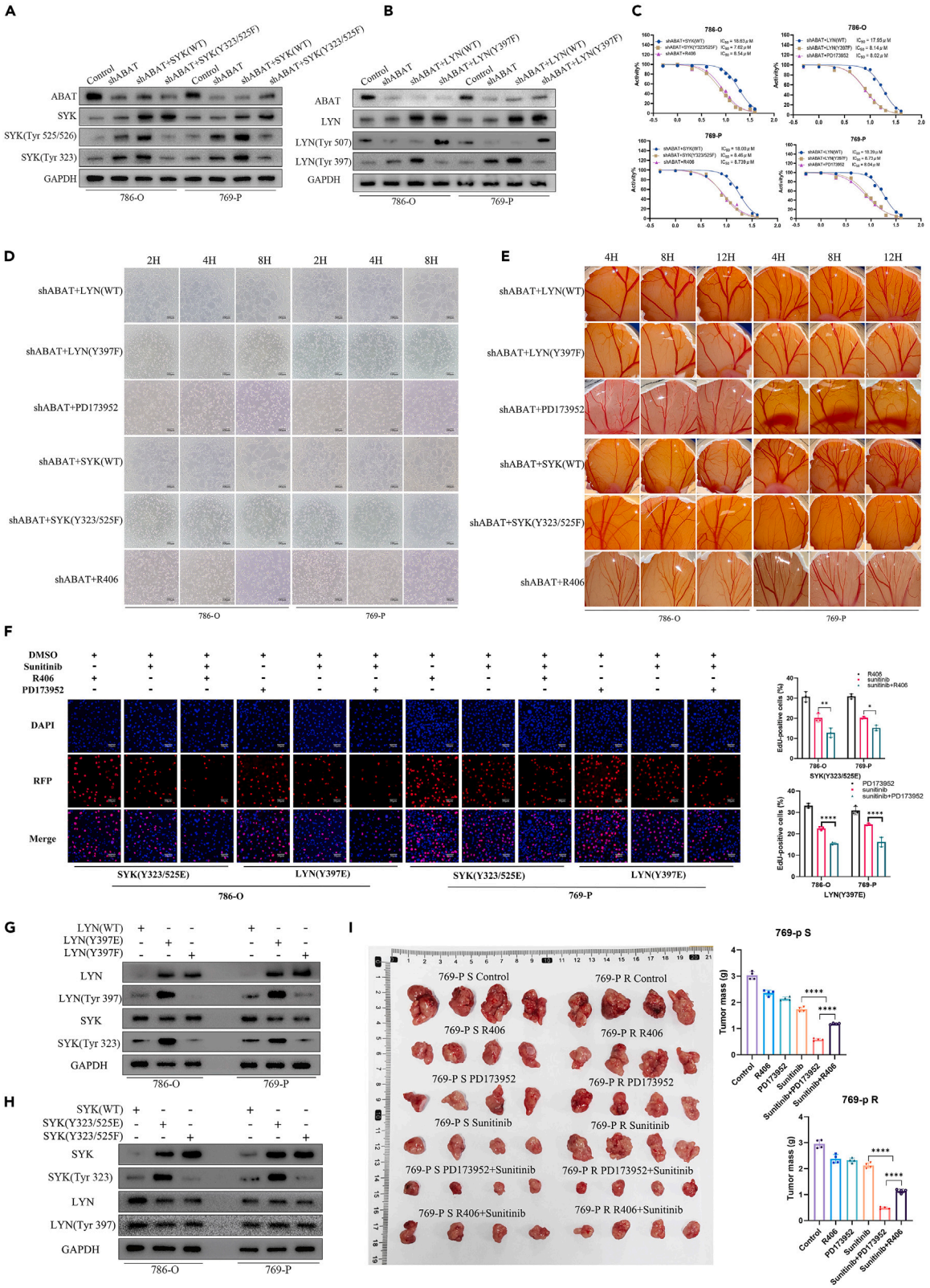
A
Control
shABAT
shABAT+SYK(WT)
shABAT+SYK(Y323/525F)
ABAT
SYK
SYK(Tyr 525/526)
SYK(Tyr 323)
GAPDH
786-O
769-P
B
Control
shABAT
shABAT+LYN(WT)
shABAT+LYN(Y397E)
ABAT
LYN
LYN(Tyr 507)
LYN(Tyr 397)
GAPDH
786-O
769-P
C
786-O
769-P
D
2H
4H
8H
shABAT+LYN(WT)
shABAT+LYN(Y397F)
shABAT+PD173952
shABAT+SYK(WT)
shABAT+SYK(Y323/525F)
shABAT+R406
786-O
769-P
E
4H
8H
12H
shABAT+LYN(WT)
shABAT+LYN(Y397F)
shABAT+PD173952
shABAT+SYK(WT)
shABAT+SYK(Y323/525F)
shABAT+R406
786-O
769-P
F
DMSO
Sunitinib
R406
PD173952
DAPI
RFP
Merge
SYK(Y323/525E)
LYN(Y397E)
786-O
769-P
R406
sunitinib
sunitinib+R406
EdU-positive cells (%)
SYK(Y323/525E)
PD173952
sunitinib
sunitinib+PD173952
LYN(Y397E)
G
LYN(WT)
LYN(Y397E)
LYN(Y397F)
LYN
LYN(Tyr 397)
SYK
SYK(Tyr 323)
GAPDH
786-O
769-P
H
SYK(WT)
SYK(Y323/525E)
SYK(Y323/525F)
SYK
SYK(Tyr 323)
LYN
LYN(Tyr 397)
GAPDH
786-O
769-P
I
769-P S Control
769-P R Control
769-P S R406
769-P R R406
769-P S PD173952
769-P R PD173952
769-P S Sunitinib
769-P R Sunitinib
769-P S PD173952+Sunitinib
769-P R PD173952+Sunitinib
769-P S R406+Sunitinib
769-P R R406+Sunitinib
769-p S
769-p R
Tumor mass (g)
Control
R406
PD173952
Sunitinib
Sunitinib+PD173952
Sunitinib+R406

Figure 5. Inhibiting LYN or SYK enhances sunitinib efficacy against resistant ccRCC

(A and B) Decreased SYK and LYN phosphorylation in ABAT-knockdown ccRCC cells (786-O and 769-P) (see Figures S7A and S7B for statistical graph).

(C) Dose-response curves and corresponding IC50 of sunitinib in ABATsh LYN^{Y397F} and ABATsh SYK$^{Y323/525F}$ ccRCC (786-O and 768-P) cells and ABATsh SYK$^{Y323/525F}$ ccRCC cells treated with R406 and ABATsh LYN^{Y397F} ccRCC cells treated with PD173952. x axis, log10 drug concentrations. y axis, Activity%, the percentage of cellular or biological activity in the drug-treated group relative to the control group.

(D) Tube formation assays of HUVECs cultured in conditioned medium from ABATsh SYK$^{Y323/525F}$, ABATsh SYK^{WT}, ABATsh treated with R406, ABATsh LYN^{Y397F}, ABATsh LYN^{WT}, or ABATsh treated with PD173952 ccRCC cells (786-O and 769-P) treated with DMSO or sunitinib for 24 h (see Figures S7C and S7D for statistical graph).

(E) Chick embryo chorioallantoic membrane (CAM) assays with conditioned medium from ABATsh SYK$^{Y323/525F}$, ABATsh SYK^{WT}, ABATsh treated with R406, ABATsh LYN^{Y397F}, ABATsh LYN^{WT}, and ABATsh treated with PD173952 ccRCC cells (786-O and 769-P) treated with DMSO or sunitinib for 24 h (see Figures S7E and S7F for statistical graph).

(F) Compared to those in the monotherapy with sunitinib, there were fewer EdU-positive cells in the combination therapy of sunitinib with R406 or PD173952 in ABATsh SYK$^{Y323/525F}$ or ABATsh LYN^{Y397F} ccRCC cells.

(G and H) Mutual interaction between SYK phosphorylation and LYN phosphorylation. Representative blots (n = 3 experiments) are shown (see Figures S7G and S7H for statistical graph).

(I) Treatments were combined with vehicle (vegetable oil), sunitinib (40 mg/kg in vegetable oil), R406 (5 mg/kg PD173952 in vegetable oil), a combination of sunitinib and R406 (40 mg/kg sunitinib and 5 mg/kg PD173952 in vegetable oil), a combination of sunitinib and PD173952 (40 mg/kg sunitinib and 20 mg/kg PD173952 in vegetable oil), or PD173952 (20 mg/kg PD173952 in vegetable oil) separately in heterograft tumors (769-P S, 769-P R cells), and tumor growth was recorded (n = 4/group) (see Figures S7I and S7J for statistical graph). The data are presented as the means ± SEMs. Groups were compared using one-way ANOVA with Tukey's multiple comparisons test, two-way ANOVA with Tukey's multiple comparisons test, or unpaired t test where appropriate. Each spot represents one subject. ns, not significant; *$p < 0.05$, **$p < 0.01$, ****$p < 0.0001$. See also Figure S7.

conducting KEGG enrichment analysis (Figure 6C), we found that these genes were predominantly enriched in the PI3K-Akt-mTOR pathway and Jak-STAT pathway. Furthermore, previous reports have indicated interactions between the changes in SYK and LYN phosphorylation and between the PI3K-Akt-mTOR pathway and the Jak-STAT pathway.[32–35]

We observed a significant increase in the phosphorylation of the AKT, mTOR, STAT3, and STAT5 genes in cells with elevated LYN (Figures 6E and S8B) and SYK phosphorylation (Figures 6F and S8C), as did the upregulation of the HIF1A protein. HIF1A was also identified during the screening of resistance-related genes. By using LYN (Figures 6D and S8A) or SYK inhibitors (Figures 6G and S8D), we successfully reduced the phosphorylation levels of AKT, mTOR, STAT3, and STAT5 activated by SYK and LYN phosphorylation and decreased the protein level of HIF1A.

Elevated phosphorylation levels of SYK and LYN upregulate PGF to promote angiogenesis

Considering the effect of SYK and LYN phosphorylation on the antiangiogenic effects of sunitinib, we further conducted an intersection analysis between genes enriched in the major altered pathways identified through KEGG enrichment analysis and genes associated with blood vessels. This analysis revealed 94 DEGs related to blood vessels (Figure 7A). Using Cytoscape software, we selected the 15 key genes and constructed a protein-protein interaction (PPI) network (Figure 7B). We selected the five genes (Figure S10H) with the greatest increase in transcription levels (Figure 7C) and investigated the changes in their protein levels following alterations in SYK and LYN phosphorylation. Notably, the protein levels of EREG and placental growth factor (PGF) were found to be positively correlated with the phosphorylation levels of LYN and SYK (Figures 7F, 7G, S9C, and S9D), and the use of LYN and SYK inhibitors (Figures 7D, 7E, S9A, and S9B) resulted in a reduction in the protein levels of EREG and PGF.

To validate the relationship between EREG and PGF and the antiangiogenic effects of sunitinib, we manipulated the expression levels of EREG and PGF in the 786-O ABATsh and 769-ABATsh cell lines (Figures 7H, 7I, S10A, and S10B). After treating the cells with sunitinib for 24 h, we collected the conditioned medium and separately cultured HUVECs (Figures 7J, S10C, and S10D) and chick chorioallantoic membrane (Figures 7K and S10E–S10G). We observed that downregulating the protein level of PGF significantly enhanced the antiangiogenic effects of sunitinib under ABAT knockdown conditions.

DISCUSSION

Cancer is a disease characterized by uncontrolled cell growth. A considerable amount of energy is required during tumor development.[36,37] ccRCC is a malignant tumor caused by genetic mutations. The Warburg effect commonly occurs through the reliance of cells on glycolysis for energy production.[38] This metabolic shift not only provides energy and synthesis for the tumor itself[39,40] but also allows the tumor to adapt to low-oxygen environments. Under hypoxic conditions, the hypoxia signaling pathway triggers angiogenesis to promote tumor cell proliferation.[41] Understanding the metabolic alterations in ccRCC and their impact on tumor growth is crucial for developing effective treatments. Current research has focused on the reprogramming of glucose, lipid, and amino acid metabolism and its effects on ccRCC. Previous studies have investigated multiple metabolic pathways to identify key genes associated with metabolism and develop a prognostic model. These genes have significant implications for patient prognosis.

One of the first-line treatments for RCC is sunitinib,[2] which blocks VEGFR and PDGFR to inhibit tumor angiogenesis and growth. However, inhibition of angiogenesis leads to a hypoxic tumor environment. Hypoxia activates the HIF family, promoting tumor angiogenesis and growth and triggering metabolic changes to cope with oxygen deficiency. Consequently, disease progression often occurs 6–15 months after sunitinib treatment.

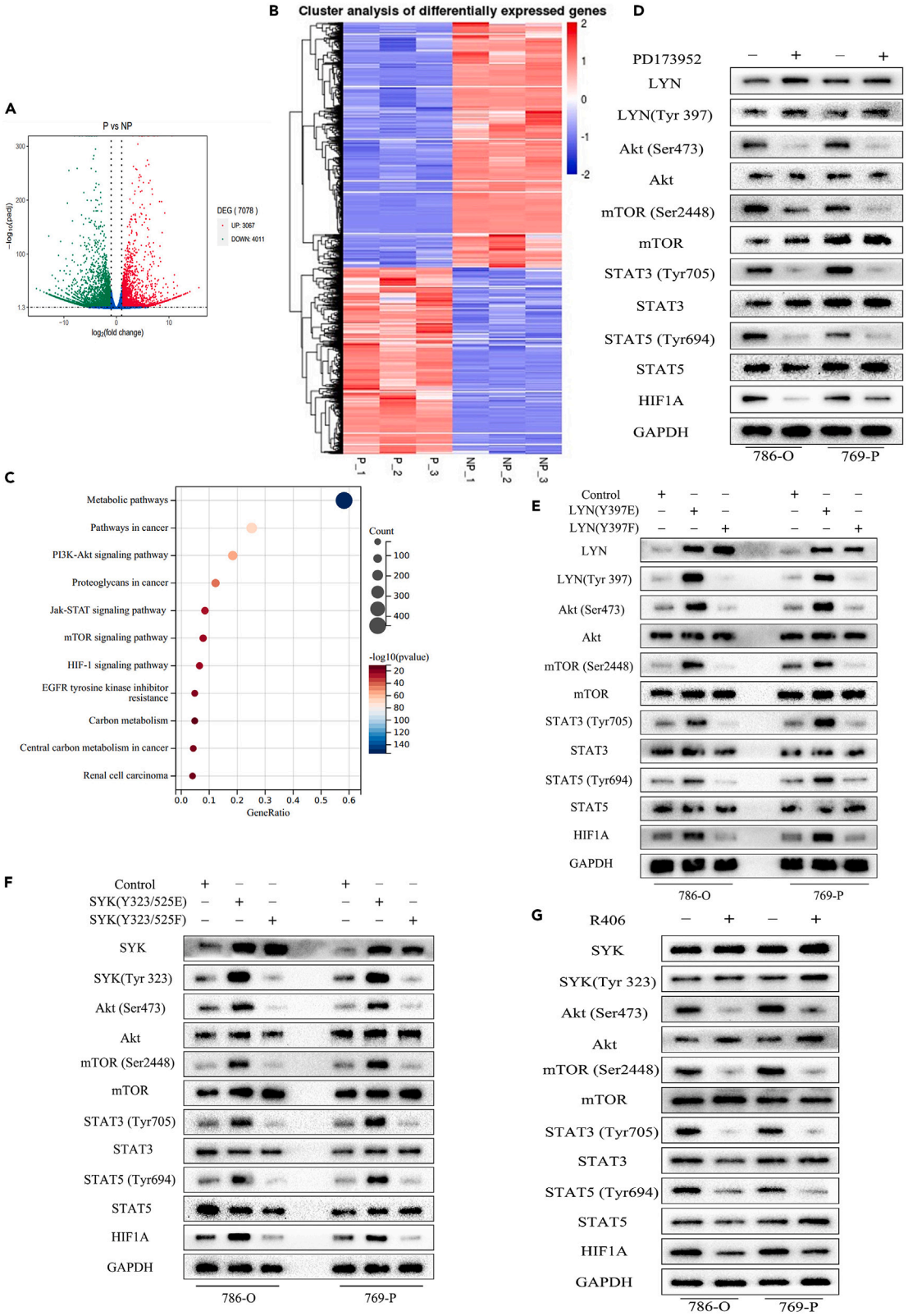
A
P vs NP
DEG (7078)
UP: 3067
DOWN: 4011
log2(fold change)
B
Cluster analysis of differentially expressed genes
P_1
P_2
P_3
NP_1
NP_2
NP_3
C
Metabolic pathways
Pathways in cancer
PI3K-Akt signaling pathway
Proteoglycans in cancer
Jak-STAT signaling pathway
mTOR signaling pathway
HIF-1 signaling pathway
EGFR tyrosine kinase inhibitor resistance
Carbon metabolism
Central carbon metabolism in cancer
Renal cell carcinoma
Count
-log10(pvalue)
GeneRatio
D
PD173952
LYN
LYN(Tyr 397)
Akt (Ser473)
Akt
mTOR (Ser2448)
mTOR
STAT3 (Tyr705)
STAT3
STAT5 (Tyr694)
STAT5
HIF1A
GAPDH
786-O
769-P
E
Control
LYN(Y397E)
LYN(Y397F)
LYN
LYN(Tyr 397)
Akt (Ser473)
Akt
mTOR (Ser2448)
mTOR
STAT3 (Tyr705)
STAT3
STAT5 (Tyr694)
STAT5
HIF1A
GAPDH
786-O
769-P
F
Control
SYK(Y323/525E)
SYK(Y323/525F)
SYK
SYK(Tyr 323)
Akt (Ser473)
Akt
mTOR (Ser2448)
mTOR
STAT3 (Tyr705)
STAT3
STAT5 (Tyr694)
STAT5
HIF1A
GAPDH
786-O
769-P
G
R406
SYK
SYK(Tyr 323)
Akt (Ser473)
Akt
mTOR (Ser2448)
mTOR
STAT3 (Tyr705)
STAT3
STAT5 (Tyr694)
STAT5
HIF1A
GAPDH
786-O
769-P

Figure 6. Elevated phosphorylation levels of SYK and LYN activate the Akt and STAT pathways

(A and B) Differential gene expression analysis of wild-type ccRCC cells and stable SYK- and LYN-phosphorylated ccRCC cell activation by sequencing.

(C) KEGG enrichment analysis of the DEGs.

(D) Western blot of key genes enriched in the pathway in LYN^{Y397E} ccRCC cells (786-O and 769-P) treated with PD173952 (see Figure S8A for statistical graph). Representative blots (n = 3 experiments) are shown.

(E) Western blot of key genes enriched in the pathway comprising LYN^{Y397E} or LYN^{Y397F} in ccRCC cells (786-O and 769-P) (see Figure S8B for statistical graph). Representative blots (n = 3 experiments) are shown.

(F) Western blot of key genes enriched in the pathway in $SYK^{Y323/525E}$ or $SYK^{Y323/525F}$ ccRCC cells (786-O and 769-P) (see Figure S8C for statistical graph). The data represent one of two independent experiments.

(G) Western blot of key genes enriched in the pathway in $SYK^{Y323/525E}$ ccRCC cells (786-O and 769-P) treated with R406 (see Figure S8D for statistical graph). Representative blots (n = 3 experiments) are shown. The data are presented as the means ± SEMs. Groups were compared using two-way ANOVA with Tukey's multiple comparisons test. Each spot represents one subject. POS, positive control spot; ns, not significant; ****$p < 0.0001$. See also Figure S8.

Various mechanisms of sunitinib resistance have been studied, including upregulation of the angiogenesis pathway, recruitment of BMDCs, enhancement of tumor invasiveness or metastasis, and activation of alternative signaling pathways. Tumor hypoxia and the accumulation of HIF1A due to various factors play crucial roles in all these processes. Therefore, the use of mTOR inhibitors to prevent HIF1 accumulation has proven effective. However, combining everolimus and sunitinib leads to significant toxicity. An alternative approach to overcoming sunitinib resistance involves combination therapy targeting a wider range of angiogenesis factors, but this approach may result in severe toxicity, making this approach impractical.

From a different perspective, tumor growth is complexly linked to nutrient metabolism, and alterations in metabolism underlie tumor adaptation to hypoxia, sustained growth, and metastasis. This phenomenon has generated significant interest among researchers. In the glucose metabolism pathway, activation of the key enzyme PCK2[42] has been found to restore the epigenetic silencing of gluconeogenesis and enhance sensitivity to sunitinib by inducing endoplasmic reticulum stress in RCC. Furthermore, in RCC, increased levels of the TKTL-1 protein promote nonoxidative sugar metabolism,[43] whereas inhibition of the glycolytic enzyme PFBFBP4 can counteract resistance to sunitinib.[44] In terms of lipid metabolism, the accumulation of cholesterol in RCC cells contributes to sunitinib resistance.[45,46] Abnormal expression of the glutamine transporter protein SLC1A5 affects intracellular glutamine metabolism,[47] leading to resistance to sunitinib. Additionally, downregulation of argininosuccinate synthase 1 (ASS1), a rate-limiting enzyme in arginine synthesis, is associated with tumor resistance in ccRCC.[48,49] However, it is important to recognize the complex interplay of life, in which sugar, fat, and amino acid metabolism are interdependent and cannot function independently. Therefore, metabolic reprogramming was considered a holistic concept in this study, aiming to identify key factors contributing to sunitinib resistance. As a result, this study explored significant alterations in key metabolic genes after sunitinib treatment and identified ABAT as a key factor. The study revealed a gradual decrease in ABAT levels during the development of sunitinib-resistant strains and demonstrated a reduction in ABAT levels after sunitinib treatment in xenograft tumors in nude mice. These changes in ABAT were closely associated with sunitinib resistance.

GABA is a signaling molecule that exhibits receptor expression not only in neural tissues but also in various organ tissues throughout the body. Furthermore, GABA serves as both an inhibitory neurotransmitter and a metabolic regulator.[50] During hypoxia, cells slow down or stop the degradation of GABA and rapidly increase its levels to help cells cope with the hypoxic environment.[51] ABAT is a critical enzyme involved in the breakdown of GABA.[52] ABAT abnormalities can lead to disrupted GABA metabolism. GABA-B receptors, which are GPCRs, play a crucial role in cellular signal transduction. Additionally, there are reports suggesting that GPCRs can transactivate tyrosine kinase receptors.[28,29]

Our research findings suggest that a decrease in ABAT leads to a decrease in sensitivity to sunitinib and a weakened inhibition of angiogenesis. Additionally, the use of GABA-B receptor agonists has similar effects. Therefore, we utilized a tyrosine kinase microarray to investigate the changes in tyrosine kinase phosphorylation after ABAT was reduced and GABA-B receptors were activated. Our results showed that the tyrosine kinases SYK and LYN were phosphorylated and activated, and these changes were blocked in cells with reduced ABAT when SYK or LYN was used. It is apparent that the activation of the G-protein-coupled receptor GABA-B subsequently activates SYK and LYN. SYK and LYN are highly expressed in ccRCC. A decrease in ABAT levels through the GABAergic system activates SYK and LYN via phosphorylation. The regulation of SYK and LYN phosphorylation has a significant impact on sensitivity to sunitinib and on antiangiogenic effects. Furthermore, inhibiting the phosphorylation of SYK and LYN effectively reversed the sunitinib resistance caused by ABAT depletion. By reviewing previous studies, we observed distinct roles of SYK and LYN in various types of cancer. In ovarian cancer, SYK plays a role in the early stages of tumor spread,[53,54] whereas in breast cancer, SYK promotes the integrity of the mammary epithelium, thereby inhibiting breast cancer invasion,[55,56] while LYN facilitates breast tumor invasion and metastasis *in vivo*.[57] In lung cancer, the absence of SYK mRNA expression is pivotal for angiogenesis,[58] and enhanced Lyn activity contributes to the development of lung cancer.[59] We also observed that the phosphorylation and activation of LYN and SYK play significant roles in sunitinib resistance in ccRCC.

Further sequencing revealed that phosphorylated SYK and LYN activate the AKT and STAT pathways, which leads to the accumulation of HIF1A. According to our angiogenesis-related gene screening, we observed a significant increase in PGF and EREG. By regulating the expression of these two vascular-related genes, we discovered that PGF plays a primary role in angiogenesis. Placental growth factor (PGF), a homolog of VEGF, binds to VEGFR-1 expressed by various cell types, including tumor cells, endothelial cells, bone-marrow-derived proangiogenic cells, inflammatory cells, and stromal cells (e.g., fibroblasts).[60,61] PGFs have various mechanisms

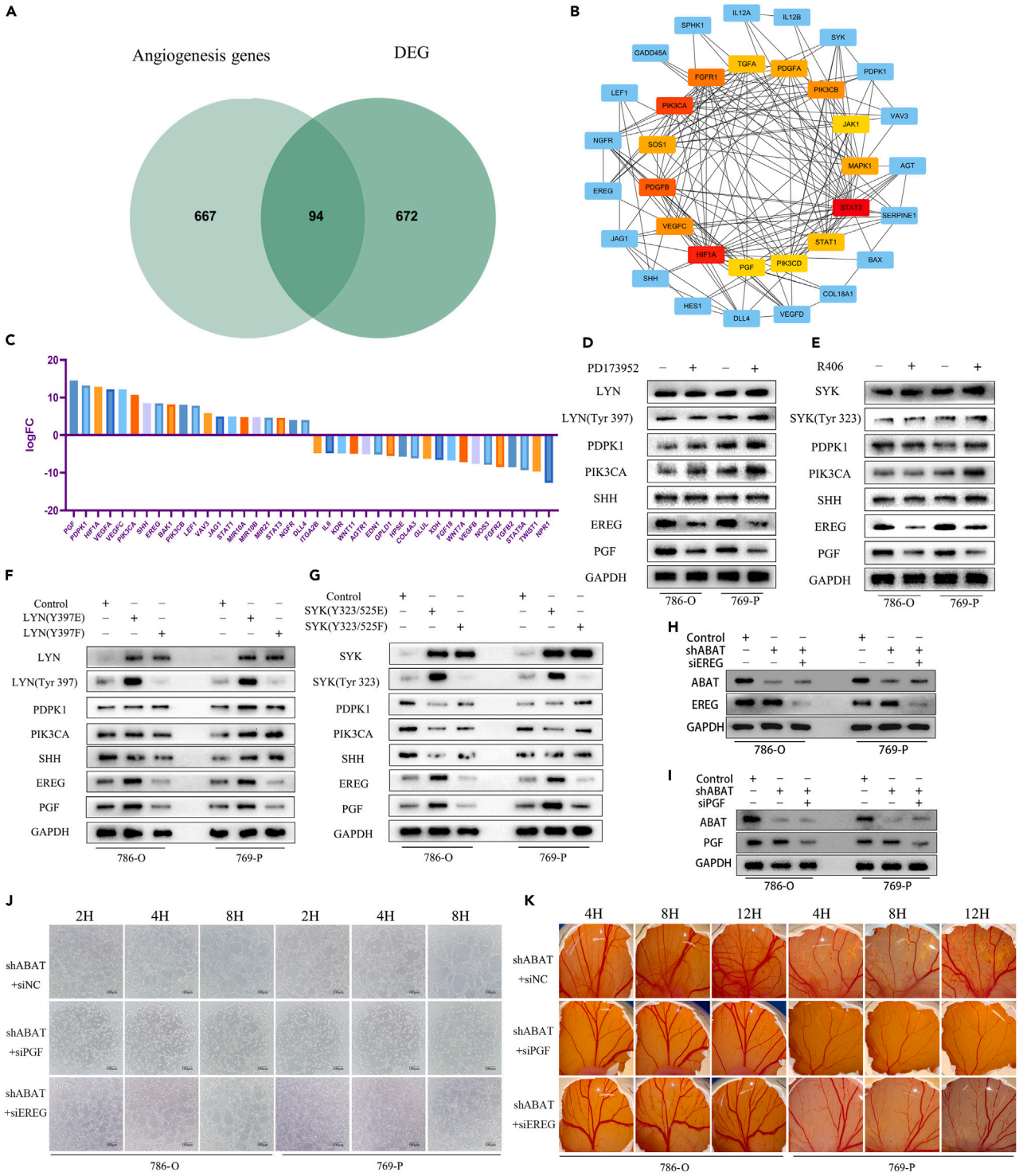

Figure 7. Elevated phosphorylation levels of SYK and LYN upregulate PGF to promote angiogenesis

(A–C) The intersection of angiogenesis genes and key genes enriched in the pathway (A). (B) A protein-protein interaction (PPI) network of the top 15 key genes from (A) was constructed. Partial vascular-related key genes (C).

(D) Western blot of PDPK1, PIK3CA, SHH, EREG, and PGF in ccRCC cells (786-O and 769-P) treated with PD173952 (see Figure S9A for statistical graph). The data represent one of two independent experiments.

(E) Western blot of PDPK1, PIK3CA, SHH, EREG, and PGF in ccRCC cells (786-O and 769-P) treated with R406 (see Figure S9B for statistical graph). The data represent one of two independent experiments.

Figure 7. *Continued*

(F) Western blot of PDPK1, PIK3CA, SHH, EREG, and PGF in LYN^{Y397E} or LYN^{Y397F} ccRCC cells (786-O and 769-P) (see Figure S9C for statistical graph). The data represent one of two independent experiments.

(G) Western blot of PDPK1, PIK3CA, SHH, EREG, and PGF in $SYK^{Y323/525E}$ or $SYK^{Y323/525F}$ ccRCC cells (786-O and 769-P) (see Figure S9D for statistical graph). The data represent one of two independent experiments.

(H and I) Inhibited EREG or PGF in ABAT-knockdown ccRCC cells (786-O and 769-P) (see Figures S10A and S10B for statistical graph).

(J) Tube formation assays using HUVECs cultured in CM from ABATsh PGFsi, ABATsh EREGsi, and ABATsh NCsi ccRCC cells (786-O and 769-P) treated with DMSO or sunitinib for 24 h (see Figures S10C and S10D for statistical graph).

(K) Chick embryo chorioallantoic membrane (CAM) assays with conditioned medium from ABATsh PGFsi, ABATsh EREGsi, and ABATsh NCsi ccRCC cells (786-O and 769-P) treated with DMSO or sunitinib for 24 h (see Figures S10E–S10G for statistical graph). The data are presented as the means ± SEMs. Groups were compared using one-way ANOVA with Tukey's multiple comparisons test, two-way ANOVA with Tukey's multiple comparisons test, or unpaired t test where appropriate. Each spot represents one subject. NC, negative control. $^{**}p < 0.01$, $^{***}p < 0.0001$, $^{****}p < 0.0001$. See also Figures S9 and S10.

for promoting angiogenesis.[60] The expression of PGF is upregulated during VEGF-targeted treatment,[62,63] which is consistent with our observed results.

In summary, we investigated the changes in key metabolic genes associated with sunitinib resistance from the perspective of metabolic reprogramming. Our findings indicate that alterations in the metabolic gene ABAT modulate the phosphorylation of SYK and LYN through the GABAergic system, thereby promoting sunitinib resistance. By combining sunitinib with an LYN inhibitor, we aimed to disrupt the resistance pathway triggered by metabolic changes induced by sunitinib treatment. This strategy can be compared to cutting off the enemy's reinforcements and supplies, ultimately prolonging the efficacy of sunitinib treatment.

Limitations of the study

Although we demonstrated the efficacy of combined treatment with sunitinib and LYN inhibitors on ABAT-downregulated tumors in nude mice xenografts, further validation is necessary in orthotopic and metastatic models of RCC before progressing to clinical trials. Metabolic reprogramming in RCC involves a wide range of genes, and this study focused on investigating one of the most significantly altered metabolic genes to elucidate the mechanism of sunitinib resistance. However, numerous other metabolism-related genes exhibiting substantial changes in expression remain unexplored, and future research will continue to investigate the mechanisms of metabolic reprogramming in RCC resistance.

STAR★METHODS

Detailed methods are provided in the online version of this paper and include the following:

- KEY RESOURCES TABLE
- RESOURCE AVAILABILITY
  - Lead contact
  - Materials availability
  - Data and code availability
- EXPERIMENTAL MODEL AND STUDY PARTICIPANT DETAILS
  - Cell lines
  - *In vivo* animal studies
- METHOD DETAILS
  - Cell
  - siRNA transfection
  - Lentivirus infection and plasmid transfection
  - Dot blotting
  - Western blotting
  - Immunofluorescence analysis
  - Chicken chorioallantoic membrane (CAM) assay
  - Human umbilical vein endothelial cell (HUVEC) tubule formation assay
  - Xenograft mouse model
  - Immunohistochemical (IHC) analysis
  - EdU incorporation assay
  - Human RTK microarray detection
- QUANTIFICATION AND STATISTICAL ANALYSIS

SUPPLEMENTAL INFORMATION

Supplemental information can be found online at https://doi.org/10.1016/j.isci.2024.110415.

ACKNOWLEDGMENTS

This study was supported by the National Natural Science Foundation of China (Grant no. 82002718); the Jiangsu Natural Science Foundation (Grant no. BK20191077); Jiangsu Province Capability Improvement Project through Science, Technology and Education (Grant no. ZDXK202219); and the National Natural Science Foundation of China (Grant no. 82372850).

AUTHOR CONTRIBUTIONS

J.L., C.L., P.S., Q. Zhang, Y.Y., and L.D. contributed to the overall study design and wrote the paper. Q. Zhang and Q. Zhai performed experiments. Q. Zhang, L.D., and Q. Zhai performed bioinformatic analyses. Z.G., Y.L., Z.T., C.N., and P.Z. assisted with the experiments. Q. Zhai, Q. Zhang, and L.D. performed animal experiments. Z.S., J.Q., P.H., and P.L. commented on the study and revised the manuscript. All authors contributed to data interpretation, discussion of results, and commented on the manuscript.

DECLARATION OF INTERESTS

The authors declare no competing interests.

Received: February 16, 2024
Revised: May 13, 2024
Accepted: June 27, 2024
Published: June 28, 2024

REFERENCES

1. Hsieh, J.J., Purdue, M.P., Signoretti, S., Swanton, C., Albiges, L., Schmidinger, M., Heng, D.Y., Larkin, J., and Ficarra, V. (2017). Renal cell carcinoma. Nat. Rev. Dis. Primers *3*, 17009. https://doi.org/10.1038/nrdp.2017.9.
2. Jin, J., Xie, Y., Zhang, J.S., Wang, J.Q., Dai, S.J., He, W.F., Li, S.Y., Ashby, C.R., Jr., Chen, Z.S., and He, Q. (2023). Sunitinib resistance in renal cell carcinoma: From molecular mechanisms to predictive biomarkers. Drug Resist. Updat. *67*, 100929. https://doi.org/10.1016/j.drup.2023.100929.
3. Joosten, S.C., Hamming, L., Soetekouw, P.M., Aarts, M.J., Veeck, J., van Engeland, M., and Tjan-Heijnen, V.C. (2015). Resistance to sunitinib in renal cell carcinoma: From molecular mechanisms to predictive markers and future perspectives. Biochim. Biophys. Acta *1855*, 1–16. https://doi.org/10.1016/j.bbcan.2014.11.002.
4. Baldewijns, M.M., van Vlodrop, I.J., Schouten, L.J., Soetekouw, P.M., de Bruine, A.P., and van Engeland, M. (2008). Genetics and epigenetics of renal cell cancer. Biochim. Biophys. Acta *1785*, 133–155. https://doi.org/10.1016/j.bbcan.2007.12.002.
5. Banks, R.E., Tirukonda, P., Taylor, C., Hornigold, N., Astuti, D., Cohen, D., Maher, E.R., Stanley, A.J., Harnden, P., Joyce, A., et al. (2006). Genetic and epigenetic analysis of von Hippel-Lindau (VHL) gene alterations and relationship with clinical variables in sporadic renal cancer. Cancer Res. *66*, 2000–2011. https://doi.org/10.1158/0008-5472.CAN-05-3074.
6. Motzer, R.J., Michaelson, M.D., Redman, B.G., Hudes, G.R., Wilding, G., Figlin, R.A., Ginsberg, M.S., Kim, S.T., Baum, C.M., DePrimo, S.E., et al. (2006). Activity of SU11248, a multitargeted inhibitor of vascular endothelial growth factor receptor and platelet-derived growth factor receptor, in patients with metastatic renal cell carcinoma. J. Clin. Oncol. *24*, 16–24. https://doi.org/10.1200/JCO.2005.02.2574.
7. Motzer, R.J., Rini, B.I., Bukowski, R.M., Curti, B.D., George, D.J., Hudes, G.R., Redman, B.G., Margolin, K.A., Merchan, J.R., Wilding, G., et al. (2006). Sunitinib in patients with metastatic renal cell carcinoma. JAMA *295*, 2516–2524. https://doi.org/10.1001/jama.295.21.2516.
8. Molina, A.M., Lin, X., Korytowsky, B., Matczak, E., Lechuga, M.J., Wiltshire, R., and Motzer, R.J. (2014). Sunitinib objective response in metastatic renal cell carcinoma: analysis of 1059 patients treated on clinical trials. Eur. J. Cancer *50*, 351–358. https://doi.org/10.1016/j.ejca.2013.08.021.
9. Rini, B.I., and Atkins, M.B. (2009). Resistance to targeted therapy in renal-cell carcinoma. Lancet Oncol. *10*, 992–1000. https://doi.org/10.1016/S1470-2045(09)70240-2.
10. Faivre, S., Demetri, G., Sargent, W., and Raymond, E. (2007). Molecular basis for sunitinib efficacy and future clinical development. Nat. Rev. Drug Discov. *6*, 734–745. https://doi.org/10.1038/nrd2380.
11. Pennacchietti, S., Michieli, P., Galluzzo, M., Mazzone, M., Giordano, S., and Comoglio, P.M. (2003). Hypoxia promotes invasive growth by transcriptional activation of the met protooncogene. Cancer Cell *3*, 347–361. https://doi.org/10.1016/s1535-6108(03)00085-0.
12. Mailhos, C., Modlich, U., Lewis, J., Harris, A., Bicknell, R., and Ish-Horowicz, D. (2001). Delta4, an endothelial specific notch ligand expressed at sites of physiological and tumor angiogenesis. Differentiation *69*, 135–144. https://doi.org/10.1046/j.1432-0436.2001.690207.x.
13. Patel, N.S., Li, J.L., Generali, D., Poulsom, R., Cranston, D.W., and Harris, A.L. (2005). Up-regulation of delta-like 4 ligand in human tumor vasculature and the role of basal expression in endothelial cell function. Cancer Res. *65*, 8690–8697. https://doi.org/10.1158/0008-5472.CAN-05-1208.
14. Sharma, R., Kadife, E., Myers, M., Kannourakis, G., Prithviraj, P., and Ahmed, N. (2021). Determinants of resistance to VEGF-TKI and immune checkpoint inhibitors in metastatic renal cell carcinoma. J. Exp. Clin. Cancer Res. *40*, 186. https://doi.org/10.1186/s13046-021-01961-3.
15. Zhang, Q., Ding, L., Zhou, T., Zhai, Q., Ni, C., Liang, C., and Li, J. (2022). A metabolic reprogramming-related prognostic risk model for clear cell renal cell carcinoma: From construction to preliminary application. Front. Oncol. *12*, 982426. https://doi.org/10.3389/fonc.2022.982426.
16. Chen, X., Cao, Q., Liao, R., Wu, X., Xun, S., Huang, J., and Dong, C. (2019). Loss of ABAT-Mediated GABAergic System Promotes Basal-Like Breast Cancer Progression by Activating Ca(2+)-NFAT1 Axis. Theranostics *9*, 34–47. https://doi.org/10.7150/thno.29407.
17. Lu, J., Chen, Z., Zhao, H., Dong, H., Zhu, L., Zhang, Y., Wang, J., Zhu, H., Cui, Q., Qi, C., et al. (2020). ABAT and ALDH6A1, regulated by transcription factor HNF4A, suppress tumorigenic capability in clear cell renal cell carcinoma. J. Transl. Med. *18*, 101. https://doi.org/10.1186/s12967-020-02268-1.
18. Jansen, M.P., Sas, L., Sieuwerts, A.M., Van Cauwenberghe, C., Ramirez-Ardila, D., Look, M., Ruigrok-Ritstier, K., Finetti, P., Bertucci, F., Timmermans, M.M., et al. (2015). Decreased expression of ABAT and STC2 hallmarks ER-positive inflammatory breast cancer and endocrine therapy resistance in advanced disease. Mol. Oncol. *9*, 1218–1233. https://doi.org/10.1016/j.molonc.2015.02.006.
19. Han, H., Zhou, S., Chen, G., Lu, Y., and Lin, H. (2021). ABAT targeted by miR-183-5p regulates cell functions in liver cancer. Int. J. Biochem. Cell Biol. *141*, 106116. https://doi.org/10.1016/j.biocel.2021.106116.
20. Gao, X., Jia, X., Xu, M., Xiang, J., Lei, J., Li, Y., Lu, Y., and Zuo, S. (2022). Regulation of Gamma-Aminobutyric Acid Transaminase Expression and Its Clinical Significance in Hepatocellular Carcinoma. Front. Oncol. *12*, 879810. https://doi.org/10.3389/fonc.2022.879810.
21. Yang, Q., Chu, W., Yang, W., Cheng, Y., Chu, C., Pan, X., Ye, J., Cao, J., Gan, S., and Cui, X. (2020). Identification of RNA Transcript Makers Associated With Prognosis of Kidney Renal Clear Cell Carcinoma by a Competing Endogenous RNA Network Analysis. Front.

Genet. *11*, 540094. https://doi.org/10.3389/fgene.2020.540094.
22. Watanabe, M., Maemura, K., Kanbara, K., Tamayama, T., and Hayasaki, H. (2002). GABA and GABA receptors in the central nervous system and other organs. Int. Rev. Cytol. *213*, 1–47. https://doi.org/10.1016/s0074-7696(02)13011-7.
23. Knott, E.L., and Leidenheimer, N.J. (2020). A Targeted Bioinformatics Assessment of Adrenocortical Carcinoma Reveals Prognostic Implications of GABA System Gene Expression. Int. J. Mol. Sci. *21*, 8485. https://doi.org/10.3390/ijms21228485.
24. Crudden, C., Shibano, T., Song, D., Suleymanova, N., Girnita, A., and Girnita, L. (2018). Blurring Boundaries: Receptor Tyrosine Kinases as functional G Protein-Coupled Receptors. Int. Rev. Cell Mol. Biol. *339*, 1–40. https://doi.org/10.1016/bs.ircmb.2018.02.006.
25. Liebmann, C., and Bohmer, F.D. (2000). Signal transduction pathways of G protein-coupled receptors and their cross-talk with receptor tyrosine kinases: lessons from bradykinin signaling. Curr. Med. Chem. *7*, 911–943. https://doi.org/10.2174/0929867003374589.
26. Natarajan, K., and Berk, B.C. (2006). Crosstalk coregulation mechanisms of G protein-coupled receptors and receptor tyrosine kinases. Methods Mol. Biol. *332*, 51–77. https://doi.org/10.1385/1-59745-048-0:51.
27. Makhov, P.B., Golovine, K., Kutikov, A., Teper, E., Canter, D.J., Simhan, J., Uzzo, R.G., and Kolenko, V.M. (2012). Modulation of Akt/mTOR signaling overcomes sunitinib resistance in renal and prostate cancer cells. Mol. Cancer Ther. *11*, 1510–1517. https://doi.org/10.1158/1535-7163.MCT-11-0907.
28. Kilpatrick, L.E., and Hill, S.J. (2021). Transactivation of G protein-coupled receptors (GPCRs) and receptor tyrosine kinases (RTKs): Recent insights using luminescence and fluorescence technologies. Curr. Opin. Endocr. Metab. Res. *16*, 102–112. https://doi.org/10.1016/j.coemr.2020.10.003.
29. Di Liberto, V., Mudo, G., and Belluardo, N. (2019). Crosstalk between receptor tyrosine kinases (RTKs) and G protein-coupled receptors (GPCR) in the brain: Focus on heteroreceptor complexes and related functional neurotrophic effects. Neuropharmacology *152*, 67–77. https://doi.org/10.1016/j.neuropharm.2018.11.018.
30. Thomas, S.M., and Brugge, J.S. (1997). Cellular functions regulated by Src family kinases. Annu. Rev. Cell Dev. Biol. *13*, 513–609. https://doi.org/10.1146/annurev.cellbio.13.1.513.
31. Brown, M.T., and Cooper, J.A. (1996). Regulation, substrates and functions of src. Biochim. Biophys. Acta *1287*, 121–149. https://doi.org/10.1016/0304-419x(96)00003-0.
32. Sutton, P., Borgia, J.A., Bonomi, P., and Plate, J.M. (2013). Lyn, a Src family kinase, regulates activation of epidermal growth factor receptors in lung adenocarcinoma cells. Mol. Cancer *12*, 76. https://doi.org/10.1186/1476-4598-12-76.
33. Wang, L., Kurosaki, T., and Corey, S.J. (2007). Engagement of the B-cell antigen receptor activates STAT through Lyn in a Jak-independent pathway. Oncogene *26*, 2851–2859. https://doi.org/10.1038/sj.onc.1210092.
34. Simon, M., Vanes, L., Geahlen, R.L., and Tybulewicz, V.L. (2005). Distinct roles for the linker region tyrosines of Syk in FcepsilonRI signaling in primary mast cells. J. Biol. Chem. *280*, 4510–4517. https://doi.org/10.1074/jbc.M410326200.
35. Gururajan, M., Dasu, T., Shahidain, S., Jennings, C.D., Robertson, D.A., Rangnekar, V.M., and Bondada, S. (2007). Spleen tyrosine kinase (Syk), a novel target of curcumin, is required for B lymphoma growth. J. Immunol. *178*, 111–121. https://doi.org/10.4049/jimmunol.178.1.111.
36. Lunt, S.Y., and Vander Heiden, M.G. (2011). Aerobic glycolysis: meeting the metabolic requirements of cell proliferation. Annu. Rev. Cell Dev. Biol. *27*, 441–464. https://doi.org/10.1146/annurev-cellbio-092910-154237.
37. Vazquez, A., Kamphorst, J.J., Markert, E.K., Schug, Z.T., Tardito, S., and Gottlieb, E. (2016). Cancer metabolism at a glance. J. Cell Sci. *129*, 3367–3373. https://doi.org/10.1242/jcs.181016.
38. Fu, Q., Xu, L., Wang, Y., Jiang, Q., Liu, Z., Zhang, J., Zhou, Q., Zeng, H., Tong, S., Wang, T., et al. (2019). Tumor-associated Macrophage-derived Interleukin-23 Interlinks Kidney Cancer Glutamine Addiction with Immune Evasion. Eur. Urol. *75*, 752–763. https://doi.org/10.1016/j.eururo.2018.09.030.
39. Jonasch, E., Walker, C.L., and Rathmell, W.K. (2021). Clear cell renal cell carcinoma ontogeny and mechanisms of lethality. Nat. Rev. Nephrol. *17*, 245–261. https://doi.org/10.1038/s41581-020-00359-2.
40. Cassim, S., Raymond, V.A., Dehbidi-Assadzadeh, L., Lapierre, P., and Bilodeau, M. (2018). Metabolic reprogramming enables hepatocarcinoma cells to efficiently adapt and survive to a nutrient-restricted microenvironment. Cell Cycle *17*, 903–916. https://doi.org/10.1080/15384101.2018.1460023.
41. Keith, B., Johnson, R.S., and Simon, M.C. (2011). HIF1α and HIF2α: sibling rivalry in hypoxic tumour growth and progression. Nat. Rev. Cancer *12*, 9–22. https://doi.org/10.1038/nrc3183.
42. Xiong, Z., Yuan, C., Shi, J., Xiong, W., Huang, Y., Xiao, W., Yang, H., Chen, K., and Zhang, X. (2020). Restoring the epigenetically silenced PCK2 suppresses renal cell carcinoma progression and increases sensitivity to sunitinib by promoting endoplasmic reticulum stress. Theranostics *10*, 11444–11461. https://doi.org/10.7150/thno.48469.
43. Langbein, S., Frederiks, W.M., zur Hausen, A., Popa, J., Lehmann, J., Weiss, C., Alken, P., and Coy, J.F. (2008). Metastasis is promoted by a bioenergetic switch: new targets for progressive renal cell cancer. Int. J. Cancer *122*, 2422–2428. https://doi.org/10.1002/ijc.23403.
44. Feng, C., Li, Y., Li, K., Lyu, Y., Zhu, W., Jiang, H., and Wen, H. (2021). PFKFB4 is overexpressed in clear-cell renal cell carcinoma promoting pentose phosphate pathway that mediates Sunitinib resistance. J. Exp. Clin. Cancer Res. *40*, 308. https://doi.org/10.1186/s13046-021-02103-5.
45. Heravi, G., Yazdanpanah, O., Podgorski, I., Matherly, L.H., and Liu, W. (2022). Lipid metabolism reprogramming in renal cell carcinoma. Cancer Metastasis Rev. *41*, 17–31. https://doi.org/10.1007/s10555-021-09996-w.
46. Naito, S., Makhov, P., Astsaturov, I., Golovine, K., Tulin, A., Kutikov, A., Uzzo, R.G., and Kolenko, V.M. (2017). LDL cholesterol counteracts the antitumour effect of tyrosine kinase inhibitors against renal cell carcinoma. Br. J. Cancer *116*, 1203–1207. https://doi.org/10.1038/bjc.2017.77.
47. Sato, T., Kawasaki, Y., Maekawa, M., Takasaki, S., Morozumi, K., Sato, M., Shimada, S., Kawamorita, N., Yamashita, S., Mitsuzuka, K., et al. (2020). Metabolomic Analysis to Elucidate Mechanisms of Sunitinib Resistance in Renal Cell Carcinoma. Metabolites *11*, 1. https://doi.org/10.3390/metabo11010001.
48. Yoon, C.Y., Shim, Y.J., Kim, E.H., Lee, J.H., Won, N.H., Kim, J.H., Park, I.S., Yoon, D.K., and Min, B.H. (2007). Renal cell carcinoma does not express argininosuccinate synthetase and is highly sensitive to arginine deprivation via arginine deiminase. Int. J. Cancer *120*, 897–905. https://doi.org/10.1002/ijc.22322.
49. Chakraborty, S., Balan, M., Sabarwal, A., Choueiri, T.K., and Pal, S. (2021). Metabolic reprogramming in renal cancer: Events of a metabolic disease. Biochim. Biophys. Acta. Rev. Cancer *1876*, 188559. https://doi.org/10.1016/j.bbcan.2021.188559.
50. Yuan, D., Wu, X., Gong, B., Huo, R., Zhao, L., Li, J., Lu, G., and Gao, H. (2023). GABA Metabolism, Transport and Their Roles and Mechanisms in the Regulation of Abiotic Stress (Hypoxia, Salt, Drought) Resistance in Plants. Metabolites *13*, 347. https://doi.org/10.3390/metabo13030347.
51. Hossein-Javaheri, N., and Buck, L.T. (2021). GABA receptor inhibition and severe hypoxia induce a paroxysmal depolarization shift in goldfish neurons. J. Neurophysiol. *125*, 321–330. https://doi.org/10.1152/jn.00149.2020.
52. Billinton, A., Ige, A.O., Bolam, J.P., White, J.H., Marshall, F.H., and Emson, P.C. (2001). Advances in the molecular understanding of GABA(B) receptors. Trends Neurosci. *24*, 277–282. https://doi.org/10.1016/s0166-2236(00)01815-4.
53. Zhang, S., Deen, S., Storr, S.J., Yao, A., and Martin, S.G. (2019). Expression of Syk and MAP4 proteins in ovarian cancer. J. Cancer Res. Clin. Oncol. *145*, 909–919. https://doi.org/10.1007/s00432-019-02856-9.
54. Peng, X., Yu, M., and Chen, J. (2020). Transcriptome sequencing identifies genes associated with invasion of ovarian cancer. J. Int. Med. Res. *48*, 300060520950912. https://doi.org/10.1177/0300060520950912.
55. Muthumanickam, S., Ramachandran, B., Boomi, P., Jeyakanthan, J., Prabu, H.G., Jegatheswaran, S., and Premkumar, K. (2023). Combination of bendamustine-azacitidine against Syk target of breast cancer: an in silico study. J. Biomol. Struct. Dyn. *41*, 13950–13962. https://doi.org/10.1080/07391102.2023.2203259.
56. Kassouf, T., Larive, R.M., Morel, A., Urbach, S., Bettache, N., Marcial Medina, M.C., Merezegue, F., Freiss, G., Peter, M., Boissiere-Michot, F., et al. (2019). The Syk Kinase Promotes Mammary Epithelial Integrity and Inhibits Breast Cancer Invasion by Stabilizing the E-Cadherin/Catenin Complex. Cancers *11*, 1974. https://doi.org/10.3390/cancers11121974.
57. Fattet, L., Jung, H.Y., Matsumoto, M.W., Aubol, B.E., Kumar, A., Adams, J.A., Chen, A.C., Sah, R.L., Engler, A.J., Pasquale, E.B., and Yang, J. (2020). Matrix Rigidity Controls Epithelial-Mesenchymal Plasticity and Tumor Metastasis via a Mechanoresponsive EPHA2/LYN Complex. Dev. Cell *54*, 302–316.e7. https://doi.org/10.1016/j.devcel.2020.05.031.
58. Chuanliang, P., Yunpeng, Z., Yingtao, H., Qifeng, S., Xiaogang, Z., and Bo, C. (2016). Syk expression in non-small-cell lung cancer and its relation with angiogenesis. J. Cancer Res. Ther. *12*, 663–666. https://doi.org/10.4103/0973-1482.154082.

59. Tsantikos, E., Gottschalk, T.A., L'Estrange-Stranieri, E., O'Brien, C.A., Raftery, A.L., Wickramasinghe, L.C., McQualter, J.L., Anderson, G.P., and Hibbs, M.L. (2023). Enhanced Lyn Activity Causes Severe, Progressive Emphysema and Lung Cancer. Am. J. Respir. Cell Mol. Biol. *69*, 99–112. https://doi.org/10.1165/rcmb.2022-0463OC.

60. Loges, S., Schmidt, T., and Carmeliet, P. (2009). "Antimyeloangiogenic" therapy for cancer by inhibiting PlGF. Clin. Cancer Res. *15*, 3648–3653. https://doi.org/10.1158/1078-0432.CCR-08-2276.

61. Ribatti, D. (2011). The controversial role of placental growth factor in tumor growth. Cancer Lett. *307*, 1–5. https://doi.org/10.1016/j.canlet.2011.02.043.

62. Casanovas, O., Hicklin, D.J., Bergers, G., and Hanahan, D. (2005). Drug resistance by evasion of antiangiogenic targeting of VEGF signaling in late-stage pancreatic islet tumors. Cancer Cell *8*, 299–309. https://doi.org/10.1016/j.ccr.2005.09.005.

63. Bagley, R.G., Ren, Y., Weber, W., Yao, M., Kurtzberg, L., Pinckney, J., Bangari, D., Nguyen, C., Brondyk, W., Kaplan, J., and Teicher, B.A. (2011). Placental growth factor upregulation is a host response to antiangiogenic therapy. Clin. Cancer Res. *17*, 976–988. https://doi.org/10.1158/1078-0432.CCR-10-2687.

STAR★METHODS

KEY RESOURCES TABLE

REAGENT or RESOURCE	SOURCE	IDENTIFIER
Antibodies		
Anti-ABTA/GABA-T antibody [EPR4433]	Abcam	Cat#ab108249; RRID: AB_10862182
Anti-GABA	GeneTex	Cat#GTX125988; RRID: AB_11173015
Anti-GAPDH (14c10) Rabbit mAb	Cell Signaling Technology	Cat# 2118L; RRID: AB_561053
Phospho-LYN (Tyr397)	Cell Signaling Technology	Cat# 70926; RRID: AB_2924371
Phospho-LYN (Tyr507)	Cell Signaling Technology	Cat# 2731; RRID: AB_2138262
Anti-LYN	Cell Signaling Technology	Cat# 2732; RRID: AB_10694080
Anti-SYK	Cell Signaling Technology	Cat# 2712; RRID: AB_2197223
Phospho-SYK (Ser297)	Cell Signaling Technology	Cat# 14140; RRID: AB_2798401
Phospho-SYK (Tyr323)	Cell Signaling Technology	Cat# 2715; RRID: AB_10828096
Phospho-SYK (Tyr525/526) (C87C1)	Cell Signaling Technology	Cat# 2710; RRID: AB_2197222
Phospho-SYK (Tyr525/526)	Cell Signaling Technology	Cat# 2711; RRID: AB_2197215
Phospho-Akt (Ser473)	Cell Signaling Technology	Cat# 9271; RRID: AB_329825
Anti-Akt	Cell Signaling Technology	Cat# 9272; RRID: AB_329827
Anti-mTOR	Cell Signaling Technology	Cat# 2972; RRID: AB_330978
Phospho-mTOR (Ser2448)	Cell Signaling Technology	Cat# 2971; RRID: AB_330970
Anti-Stat3 (79D7)	Cell Signaling Technology	Cat# 4904; RRID: AB_331269
Phospho-Stat3 (Tyr705)	Cell Signaling Technology	Cat# 9131; RRID: AB_331586
Anti-Stat5 (D2O6Y)	Cell Signaling Technology	Cat# 94205; RRID: AB_2737403
Phospho-Stat5 (Tyr694)	Cell Signaling Technology	Cat# 9351; RRID: AB_2315225
Anti-HIF1-a (D2U3T) Rabbit mAb	Cell Signaling Technology	Cat# 14179; RRID: AB_2622225
Anti-PDPK1/PDK1	GeneTex	Cat# GTX50366; RRID: AB_11179547
Anti-Shh (C9C5) Rabbit mAb	Cell Signaling Technology	Cat# 2207; RRID: AB_2188191
Anti-EREG (D4O5I) Rabbit mAb	Cell Signaling Technology	Cat# 12048; RRID: AB_2797808
Anti-PLGF	GeneTex	Cat# GTX101023; RRID: AB_1951205
Anti-mouse IgG, HRP-linked	Cell Signaling Technology	Cat# 7076; RRID: AB_330924
Anti-rabbit IgG, HRP-linked	Cell Signaling Technology	Cat# 7074; RRID: AB_2099233
Anti-CD31 antibody	Abcam	Cat# ab28364; RRID: AB_726362
Chemicals, peptides, and recombinant proteins		
RPMI 1640	GIBCO	Cat# C22400500BT
Ham's F-12K	GIBCO	Cat# 21127022
FBS	GIBCO	Cat# 10091148
0.25% Trypsin-EDTA (1X)	GIBCO	Cat# 25200072
PBS PH 7.4 basic (1X)	GIBCO	Cat# C10010500BT
γ-Aminobutyric acid	Aladding	CAS: 56-12-2
Baclofen	MedChemExpress	CAS: 1134-47-0
Phaclofen	Aladding	CAS: 1140-12-3
Dimethyl sulfoxide (DMSO)	MedChemExpress	CAS: 67-68-5
Sunitinib (SU 11248)	MedChemExpress	CAS: 557795-19-4
PD173952	MedChemExpress	CAS: 305820-75-1

(*Continued on next page*)

Continued

REAGENT or RESOURCE	SOURCE	IDENTIFIER
R406	MedChemExpress	CAS: 841290-81-1
DAPI	Invitrogen	Cat# D1306
RIPA Lysis Buffer	Beyotime	Cat# P0013C
SDS-PAGE Sample Loading Buffer, 5X	Beyotime	Cat# P0015
SDS-PAGE Electrophoresis Buffer with Tris-Gly, 10X	Beyotime	Cat# P0014D
Rapid Transfer Buffer, 20X	Leapwal	Cat# ED510
CCK-8 Cell Counting Kit	Vazyme	Cat# A311-01
Trizol	Invitrogen	Cat# 15596026
Polybrene	YEASEN	CAS: 40804ES76
Immunol Fluorescence Staining Secondary Antibody Dilution Buffer	Beyotime	Cat# P0108
lipofectamine3000	ThermoFisher	Cat# L3000008
Critical commercial assays		
Human RTK Phosphorylation Antibody Array Kit	RayBiotech	Cat# AAH-PRTK-1-8
EdU incorporation assay kit	Beyotime	Cat# C0071L
Experimental models: Cell lines		
786-O	Procell Life Science & Technology	Cat# CL-0010
769-P	Procell Life Science & Technology	Cat# CL-0009
HUVEC	Procell Life Science & Technology	Cat# CL-0122
786-O SYK$^{Y323/525E}$	This paper	N/A
769-P SYK$^{Y323/525E}$	This paper	N/A
786-O LYN^{Y397E}	This paper	N/A
769-P LYN^{Y397E}	This paper	N/A
786-O LYN^{Y397F}	This paper	N/A
769-P LYN^{Y397F}	This paper	N/A
769-P SYK$^{Y323/525F}$	This paper	N/A
786-O SYK$^{Y323/525F}$	This paper	N/A
786-O^{oeABAT}	This paper	N/A
769-P^{oeABAT}	This paper	N/A
786-O^{shABAT}	This paper	N/A
769-P^{shABAT}	This paper	N/A
Experimental models: Organisms/strains		
Mouse: BALB/cNj-Foxn1nu/Gpt	Gempharmatech Co.	RRID:IMSR_GPT:D000521
Chick embryo	Nanjing Zhushun Biotechnology Co.	N/A
Oligonucleotides		
Human EREG siRNA	This paper	N/A
Human PGF siRNA	This paper	N/A
Recombinant DNA		
Plasmid: pcDNA3.1+-flag-hABAT-mCherry	This paper	N/A
Plasmid: pcDNA3.2+-flag-hSyk (Y323/525E)	This paper	N/A
Plasmid: pcDNA3.2+-flag-hSyk (Y323/525F)	This paper	N/A
Plasmid: pcDNA3.2+-flag-hSyk (wt)	This paper	N/A
Plasmid: pcDNA3.2+-flag-hLyn (Y397E)	This paper	N/A
Plasmid: pcDNA3.2+-flag-hLyn (Y397F)	This paper	N/A

(*Continued on next page*)

Continued

REAGENT or RESOURCE	SOURCE	IDENTIFIER
Plasmid: pcDNA3.2+-flag-hLyn (wt)	This paper	N/A
Plasmid: pcDNA3.3+	This paper	N/A
Plasmid: pcDNA3.1+-flag-hABAT(sh)	This paper	N/A
Software and algorithms		
GraphPadPrism8	GraphPad	https://www.graphpad.com/scientific-software/prism/
ImageJ	GitHub	https://imagej.net/software/imagej/
ImageLab	Biorad	N/A

RESOURCE AVAILABILITY

Lead contact

Further information and requests for resources and reagents should be directed to and will be fulfilled by the lead contact, Jie Li (drc_lijie@126.com).

Materials availability

This study did not generate new unique reagents. Mouse lines and plasmids generated in this study are available upon request from the lead contact.

Data and code availability

- All raw data reported in this paper will be shared by the lead contact upon request.
- This study does not report original code.
- Any additional information required to reanalyze the data reported in this paper is available from the lead contact upon request.

EXPERIMENTAL MODEL AND STUDY PARTICIPANT DETAILS

Cell lines

The human ccRCC cell lines 786-O (cat no. CL-0010) and 769-P (cat no. CL-0009), as well as the human umbilical vein endothelial cell line HUVEC, were obtained from Procell Life Science & Technology (Wuhan, China). These cell lines were authenticated by short tandem repeat profiling by Procell Life Science & Technology.

In vivo animal studies

Approval for the animal experiments was obtained from the Nanjing Medical University Animal Ethics Committee (approval no. IACUC 2209036). BALB/c nude mice aged 4-6 weeks were obtained from Jiangsu Jicui Yaokang Biotechnology Co., Ltd.

METHOD DETAILS

Cell

In addition, 769-P and 786-O cells were cultured in RPMI 1640 medium, while HUVECs were cultured in Ham's F-12K medium supplemented with 10% fetal bovine serum (FBS). All the cells were incubated at 37°C with 5% CO2. To generate sunitinib-resistant 786-O and 769-P cells, sunitinib was dissolved in DMSO at working concentrations of 10 μM, 15 μM, and 20 μM. The ccRCC cells were then maintained in sunitinib solution in RPMI 1640 medium supplemented with 10% FBS at 37°C with 5% CO2 for 2 weeks. Afterward, the cells were cultured for an additional two weeks without sunitinib. The half maximal inhibitory concentration (IC50) of sunitinib was determined in 786-O and 769-P cells, which were cultured in sunitinib conditions for two additional weeks. This process was repeated four times. The resulting cells were identified as sunitinib resistant and designated 786-O R and 769-P R. Both 786-O and S786-O cells were subsequently maintained at 37°C with 5% CO2 without sunitinib for further experiments.

siRNA transfection

PGF siRNA (siPGF), EREG siRNA (siEREG), and a negative control (siNC) were obtained from Thermo Scientific. Transfection was performed using the Lipofectamine 3000 Transfection Kit (Invitrogen).

Lentivirus infection and plasmid transfection

The cells were incubated with Lenti-CRISPR v2 (Addgene) encoding the ABAT transcript (oeABAT) and 4 mg/mL polybrene for 24 h. Puromycin (0.5 μg/mL) was added to the medium for selection. ABAT short hairpin RNA (shRNA) oligonucleotides (shRNA: 5′-GCAGCACAAGGGAATACAATC-3′) were designed and synthesized by PROTEINBIO, China, and subsequently cloned and inserted into the HindIII/EcoR1 sites of the pcDNA3.1+ vector to construct ABAT knockdown plasmids. Transfections were performed using Lipofectamine 3000 (Invitrogen, California, America) according to the manufacturer's instructions. Stably transfected cell lines were selected with 0.5 μg/mL puromycin for more than 10 days. Mutations in pcDNA3.2+-flag-hSyk $^{(Y323/525E)}$, pcDNA3.2+-flag-hSyk $^{(Y323/525F)}$, pcDNA3.2+-flag-hLyn $^{(Y397E)}$, and pcDNA3.2+-flag-hLyn $^{(Y397F)}$ were generated by site-directed mutagenesis PCR.

Dot blotting

Total crude protein was extracted from cells and tissues, and its concentration was determined using the Bradford protein assay (Bio-Rad, CA). The samples (2 μl) were spotted onto nitrocellulose membranes. The membrane spots were then air-dried and incubated at room temperature in blocking solution (5% skim milk dissolved in ultrapure water) for 1 h. After blocking, the membrane was incubated with a primary antibody solution at the appropriate dilution for 1 h at room temperature. Following washing, the membrane was incubated with a properly diluted secondary antibody solution for another 1 h at room temperature. The signal was detected using an enhanced chemiluminescence detection system (Bio-Rad, USA) as described by the manufacturer.

Western blotting

The cells and tissues were subjected to total crude protein extraction, and the concentration of total crude protein was quantified using the Bradford protein assay (Bio-Rad, CA). Subsequently, sodium dodecyl sulfate–polyacrylamide gel electrophoresis (SDS–PAGE) was conducted, and the separated proteins were transferred to a 0.45 mm pore size Immobilon-P PVDF Membrane from Millipore. Immunoblotting was used to assess protein expression, and the key resources table provides a comprehensive list of the antibodies utilized in this study.

Immunofluorescence analysis

CcRCC cells were fixed in cold 4% formaldehyde for 15 minutes, rinsed, and stored prior to analysis. Primary antibody staining was performed with a 1:500 dilution of the GABA antibody from GeneTex. After incubation, the cells were washed and incubated with a 1:2000 dilution of Alexa-conjugated secondary antibody from Life Technologies. The cells were counterstained with a 1:10,000 dilution of DAPI. Images were obtained using a fluorescence microscope from Nikon, Japan.

Chicken chorioallantoic membrane (CAM) assay

Day-5 fertilized chicken eggs from Nanjing Zhushun Biotechnology Co., Ltd., Nanjing, China, were chosen for the CAM assay. To expose the CAM, a window approximately 1.0 cm in diameter was opened in the eggshell, and then the shell membrane was gently peeled off with ophthalmic forceps to expose the chick embryo's down and amnion. The chicken embryos were randomly divided into groups, with each group containing 4 embryos. Subsequently, 100 μL of conditioned culture medium was added to the amnion through the window. The window was sealed using sterile adhesive tape, and the eggs were incubated at 37°C with 80–90% relative humidity for 2 days. Vascular changes were recorded at 12 h, 24 h, and 48 h posttreatment and analyzed using ImageJ software.

Human umbilical vein endothelial cell (HUVEC) tubule formation assay

Matrigel solution (Corning, USA) was added to a prechilled 96-well sterile plate and incubated at 37°C for 30 minutes to 1 h, after which the Matrigel was allowed to gel. HUVECs were suspended in conditioned medium obtained from ccRCC cell lines at a concentration of approximately 1–2 × 105 cells/ml. The HUVEC suspension (2–3 × 104 cells) was added to the solidified Matrigel in each well. The plate was then incubated at 37°C for 18 h. Capillary tubes were removed at 2 h, 4 h, and 8 h and analyzed using ImageJ software. Each treatment required three separate and independent experiments.

Xenograft mouse model

Animal experiments were conducted following the approval of the Animal Ethics Committee of Nanjing Medical University (acceptance no. IACUC 2209036) and in accordance with animal protocols approved by the Animal Care and Use Committee of Nanjing Medical University. Four- to six-week-old BALB/c nude mice were purchased from Jiangsu Jicui Yaokang Biotechnology Co., Ltd., to establish a xenograft tumor model. The mice were housed in laminar flow cabinets under specific pathogen-free conditions and provided unrestricted access to food and water. Xenograft tumors were generated by injecting 1×106 ccRCC cells (769-P, 786-O ABATsh, 786-O ABATsh LynY397E, or 786-O ABATsh LynY397F) subcutaneously. One week after the injection, the mice were treated with vegetable oil (control), sunitinib (40 mg/kg in vegetable oil, orally, 5 days per week), or a combination of sunitinib and PD173952 (40 mg/kg sunitinib and 20 mg/kg PD173952 in vegetable oil, orally, 5 days per week). Tumor volume was measured every 3-4 days and calculated using the formula: volume = length × (width)2/2. Four weeks after sunitinib treatment, the mice were euthanized, and the tumors were resected and weighed.

Immunohistochemical (IHC) analysis

The paraffin-embedded sections were dewaxed, rehydrated, treated to block endogenous peroxidase activity, and subjected to antigen retrieval by microwave heating. After blocking nonspecific antigen binding, the sections were incubated overnight at 4°C with specific primary antibodies against ABAT or CD31 (1:100 dilution; Abcam, USA). Following incubation with the corresponding secondary antibodies, the sections were stained with diaminobenzidine and counterstained with hematoxylin. Representative images were captured using an Olympus light microscope.

EdU incorporation assay

Transfected cells were cultured in 96-well plates at a density of 1 × 104 cells/well. The EdU incorporation assay kit (Beyotime, China) was used to evaluate cell proliferation. Images were acquired using a fluorescence microscope (Nikon, Japan).

Human RTK microarray detection

Semiquantitative detection of 71 phosphorylated human receptor tyrosine kinases (RTKs) in cell and tissue lysates was performed using the Human RTK Phosphorylation Antibody Array Kit (RayBiotech, USA) following the manufacturer's instructions.

QUANTIFICATION AND STATISTICAL ANALYSIS

Statistical analyses were conducted using GraphPad software or R, with specific experimental details, such as the tests employed and the value/definition of n, provided in the figure legends. Bar charts and error bars denote means and standard error of the mean (SEM). *In vitro* assays were conducted with 2–4 technical replicates per condition. Sample sizes for *in vivo* mouse studies were determined based on the typical number of mice required to achieve statistical significance given the variability within study arms. Each data point represents either a biological replicate (individual mouse for *in vivo* studies). Statistical significance was defined as p-values and false discovery rate (FDR) values < 0.05 in all analyses.